JOURNAL OF MATERIALS SCIENCE **40** (2005) 1–26

Review
Nano and macro-structured component fabrication by electron beam-physical vapor deposition (EB-PVD)

J. SINGH, D. E. WOLFE
Applied Research Laboratory, The Pennsylvania State University, University Park, 115 MRI Building, PA 16804, USA
E-mail: jxs46@psu.edu

The objective of this paper is to demonstrate the versatility of electron beam-physical vapor deposition (EB-PVD) technology in engineering new materials with controlled microstructure and microchemistry in the form of coatings. EB-PVD technology is being explored in forming net-shaped components for many applications including space, turbine, optical, biomedical and auto industry. Coatings are often applied on components to extend their performance and life under severe environmental conditions including thermal, corrosion, wear, and oxidation. In addition, coatings have been used in designing and developing sensors. Performance and properties of the coatings depend upon its composition, microstructure and deposition condition. This paper presents recent results of various materials including ceramic, metallic, and functionally graded coatings produced by EB-PVD. Simultaneous co-evaporation of multiple ingots of different compositions in the high energy EB-PVD chamber has brought considerable interest in the architecture of functional graded coatings, nano-laminated coatings and designing of new structural materials that could not be produced economically by conventional methods. In addition, high evaporation and condensate rate allowed fabricating precision net-shaped components with nanograined microstructure for various applications. This paper will also present the results of various metallic and ceramic coatings including chromium, titanium carbide (TiC), hafnium carbide (HfC), tantalum carbide (TaC), hafnium nitride (HfN), titanium-boron-carbonitride (TiBCN), and partially yttria stabilized zirconia (YSZ), and HfO_2-based TBC coatings deposited by EB-PVD for various applications.

1. Introduction

Coatings play an important role ranging from under-sea to space applications including communications, sensors, satellites, optics, auto, and aerospace industries [1–6]. High temperature components of gas-turbine engines for aircraft such as airfoils and vanes are coated with metallic and ceramic coatings to enhance performance and reliability [7–10]. Thus, there is a continuous effort to engineer surface properties of the material enhancing the life of components under severe environmental conditions where corrosion, high-temperature oxidation, and wear are concerns. Similarly, multilayered ceramic and metallic films are extensively used in the fabrication of microelectronic and communication components [11, 12]. It is important to understand the inter-relationship of applications, coatings and processes. Applications dictate the selection of coating materials, and the desired thermal, chemical, and mechanical properties often determine the deposition method and processing parameters [13].

Coating process can be broadly classified into three groups: vapor phase, which includes physical vapor deposition (PVD) and chemical vapor deposition (CVD); liquid phase, which-includes painting, dipping and electroplating; and solid phase which includes plasma spray processes and laser cladding [14–20]. Each process can again be sub-classified based on the source of energy used for the deposition of coatings as shown in Table I, and briefly discussed in the Appendix. Each of these processes has its advantages and disadvantages. Comparison of CVD, PVD and plasma spray processes is given in Table II [21–23]. Chemical and physical conditions during the deposition reaction can strongly affect the composition, residual stresses, and microstructure (i.e., amorphous, polycrystalline, epitaxial, and textured) of the coating. The desired coating thickness and material properties (including microstructure, physical, and mechanical properties) are dictated by its application, which will determine the coating deposition process to be used. The objective of this research

TABLE I Coating deposition techniques [14–20]

- Powder Spray deposition processes
  - Thermal spray, Plasma spray
  - High-velocity-oxy-fuel (HVOF)
  - Detonation gun (D-gun)
- Chemical vapor deposition processes (CVD)
  - Low pressure CVD
  - Plasma enhanced CVD
  - Photochemical and laser-CVD
- Physical vapor deposition processes (PVD)
  - Thermal evaporation
  - Electron beam-PVD
  - Sputtering
    - Balanced and unbalanced magnetron sputtering
    - Direct current diode sputtering
    - Radio frequency sputtering
    - Triode-assisted PVD
  - Cathodic arc
  - Ion plating

paper is to briefly review vapor phase coating growth mechanism followed by the most recent research work conducted in developing coatings/components for various applications by the electron beam-physical vapor deposition (EB-PVD) process. In addition, the usage of EB-PVD technology will demonstrate in producing near net-shaped components with controlled microstructure and chemistry.

2. Electron beam-physical vapor deposition (EB-PVD) process

EB-PVD is a simple process in which a focused high-energy electron beam is directed to melt the evaporant material(s) in a vacuum chamber (Fig. 1). The evaporating material condenses on the surface of the substrates or components resulting in the formation of deposit, i.e., coating. During deposition, external heating is often applied to the substrate for enhancing metallurgical bonding between the coating and the substrate. EB-PVD is primarily a line-of-sight process, therefore, uniform coating of complex parts (such as turbine airfoils) is accomplished by continuous rotation in the vapor cloud during the deposition process.

There are four main components in the EB-PVD unit, namely, EB-gun assembly, water cooled copper crucible which contains the material to be evaporated, the substrate (part to be coated), and the vacuum chamber unit with enhanced flexibility for a variety of coating applications. The EB gun can be self-accelerated straight or electromagnetic deflected through 180 or 270° as shown in Fig. 1. Similarly, the evaporant material is placed in a water-cooled copper crucible, which could be either pocket type for small quantity evaporation application (Fig. 1) or continuous ingot feeding through a copper-cooled crucible (Fig. 2 as marked A, B and C) for larger quantity evaporation. Flexibility in the application of EB-PVD unit can be enhanced by using many EB guns and continuous multiple ingots feeding system (Fig. 2) as discussed in the next section.

The industrial research pilot plant scale EB-PVD in the author's laboratory at Penn State University has six electron beam guns, four of which can be used to evaporate the coating material and two to preheat the substrate (either directly or indirectly) to facilitate coating adhesion, proper chemistry and microstructural control (Fig. 2). Each gun has an average power 45 kW capacity (with peak power 60 kW). The chamber accommodates up to three ingots ranging in size from 25 to 68 mm in diameter and up to 450 mm length. The overall volume of the coating chamber is approximately 1 cubic meter. The maximum diameter of the substrate with vertical rotation is about 400 mm and can be rotated at a speed of 5.5 to 110 rpm with a maximum

TABLE II Comparison between CVD, PVD, EB-PVD and plasma spray processes [21–23]

Coating process	Substrate temperature (°C)	Deposition rate	Surface roughness	Type of bonding	Typical microstructure	Coating material	Environment	Flexibility
Plasma spray	RT to 800 (flexible)	>100 μm/min	Very rough	Mechanical	Deformed-lamella	Metal, ceramic	Noise	Flexible
CVD	>800–1200 (must)	<0.08 μm/min (<5 μm/h)	Smooth	Diffusional	Columnar, Equiaxed	Metal, ceramic	Chemical gas disposal	Limited
PVD-sputtering	<600 (flexible)	<0.08 μm/min (<5 μm/h)	Smooth	Diffusional	Columnar	Metal, ceramic	Clean	Limited
EB-PVD	RT to 1200 (flexible)	.01 to 100 μm/min	Smooth	Diffusional	Columnar, nanograined equiaxed	Metal, ceramic	Clean	Flexible

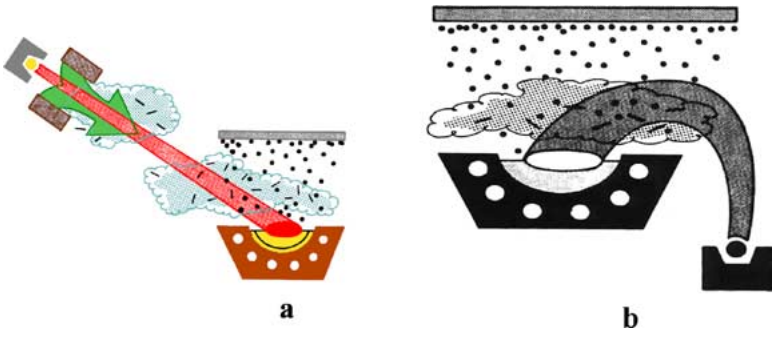

Figure 1 Schematic diagram showing: (a) straight and (b) electromagnetic deflected electron beam guns [24].

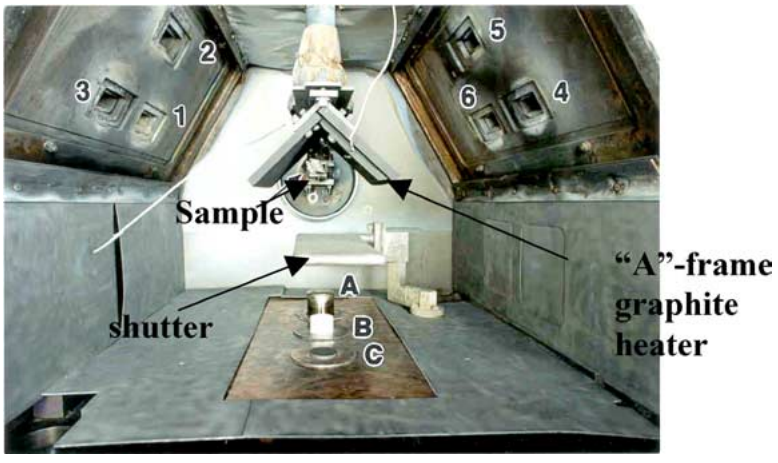

Figure 2 Photograph of the EB-PVD chamber showing six EB guns (1–6), three continuous ingot (A–C) feeding system, "A-shaped" graphite heater, deposition shutter, and rotating sample between the graphite heater and the deposition shutter.

load capacity of 100 Kg. The unit also has a horizontal sample holder with a three-axis part manipulator: two rotary axes of 0–14 rpm and a 0–4000 mm/min translation axis. It can accommodate samples weighing up to 20 kg.

The EB-PVD process offers extensive possibilities for controlling variations in the structure and composition of the processed materials. For example, coating compositions can be varied continuously, in the so-called Functional Graded Coatings (FGC). Coatings can be graded from metallic to metallic, ceramic to ceramic, metallic to ceramic, or ceramic to metallic depending on what is desired [25–27]. Also, multilayer coatings comprising of alternating layers of different compositions including metals, ceramics, and polymers can be made on a variety of substrates, depending on the desired application [28, 29]. The EB-PVD process offers many desirable characteristics such as relatively high deposition rates (up to 150 μm/min with an evaporation rate of $\sim$10–15 Kg/h), dense coatings, controlled composition, tailored microstructure, low contamination, and flexible deposition parameters [27, 28]. Coatings produced by the EB-PVD process usually have a good surface finish and a uniform microstructure. The microstructure and composition of the coating can be easily altered by manipulating the process parameters and ingot compositions. Thus, multilayered ceramic/metallic coatings can be readily formed and various metallic and ceramic coatings (oxides, carbides, and nitrides) can be deposited at relatively low temperatures. Even elements with low vapor pressure such as molybdenum, tungsten, rhenium and carbon are readily evaporated by this process.

Two ion sources (8 cm Kaufman and Endhall) are periodically used in the EB-PVD unit to modify the microstructure, properties and chemistry of the deposited coating. Depending on the desired coating properties, the high-energy gridded 8 cm Kaufman or low-energy (high current) Endhall ion beam source is used. The attachment of the ion beam source to the EB-PVD unit offers two additional features. The substrate surface can be ion beam sputter cleaned/etched prior to deposition to promote adhesion between the coating and the substrate or during deposition to produce the desired microstructure and chemistry as discussed briefly below [30–43].

2.1. Ion beam etching and pre-cleaning

The function of ion beam etching or pre-cleaning the substrate is the same. In ion beam etching, an ionized beam of gas is directed towards the substrate's surface, prior to deposition, to remove contamination material. This removal of surface material is the result of physical sputtering of the material from the surface due to the momentum transfer between the energetic beam atoms and the substrate surface atoms. Generally, for physical sputtering, an inert gas, such as argon, is used. Bombardment of the substrate surface prior to deposition (i.e., sputter cleaning) promotes better adhesion. The two major effects occurring during this pre-cleaning step are: (1) removal of adsorbed hydrocarbons and water molecules and (2) increasing the density of nucleation sites for condensation [35, 38]. Not removing these materials /molecules prior to deposition results in poor adhesion as they serve as weak links for bonding. Thus, *in-situ* ion beam cleaning of samples prior to coating deposition is often used during these efforts.

2.2. Microstructure and property enhancement

In the last several years, ion beams have gained increased importance during the deposition process to enhance the properties of the depositing film. Ion bombardment of the substrate occurs while the source material is evaporated by either resistance or EB. The state of the internal stresses developed in the coating can be changed from tensile to compressive stress by the forcible injection of high-energy atoms (i.e., ion implantation). Thus the ability to control the stress level is an additional feature of the ion beam assisted deposition (IBAD) process [39–49]. Chemical vapor deposited coatings generally form with tensile stresses due to the thermal expansion mismatch with the substrate, which often limit the coating thickness before spallation occurs. Ion bombardment during deposition

has a tendency to reduce the tensile stress and often changes the intrinsic stress from tensile to compressive [41–49]. Depending on the energy of the ion beam, texturing or preferred crystal growth orientation can be controlled [50–60]. IBAD can be used to change optical properties and decrease the permeability of water by increasing the density of the deposited film. Changes in the crystal structure of the film have also been reported with IBAD. For example, the microstructure of ZrO_2 has been changed from amorphous to polycrystalline using IBAD [61]. In addition, the morphology of molybdenum films deposited on silicon were shown to change from columnar to isotropic due to ion bombardment [44]. In addition, numerous authors have reported increases in the average hardness of coatings deposited with IBAD [38, 62–66]. The increase in hardness is obtained by increasing the density, decreasing grain size, changing stress state, and controlling the crystallographic texture of the coating. Improved step coverage (i.e., high surface roughness or complex geometries) has also been reported when using IBAD [67]. This is most likely the result of increased atom mobility under bombardment.

In addition, ion beams are used in synthesizing coatings by reacting the evaporant with the ionized reactive gases including nitrogen, oxygen, methane and acetylene. Ionized gas chemically reacts with the vapor cloud forming alloyed coatings such as nitrides of Hf, Ti, Zr; carbides of Ti, Hf, Ta, and Zr, and oxides of Zr and Al.

The choice of the deposition technique is determined by the application for the coating, the desired coating properties, temperature limitation of the substrate, uniformity or consistency of the process, and its compatibility with subsequent processing steps. Chemical and physical conditions during the deposition reaction can strongly affect the resultant microstructure of the coating (i.e., single-crystalline, polycrystalline, amorphous, epitaxial). Multilayered metallic or ceramic coatings are often applied on the components to achieve the desired properties. Properties and performance of the coating are heavily dependent upon the coating microstructure. It has been well established that multilayered coatings with the layer thickness of <1 μm offer superior structural and physical properties due to refined microstructure in the coating [68–70]. In all vapor-phase coating processes including CVD and PVD, the basic mechanisms of coating growth are very similar, therefore it is important to briefly review thin film growth mechanisms.

3. Nucleation and growth mechanisms of thin films

The films growth mechanism remains the same as deposited by either CVD or PVD including sputtering and EB-PVD. Significant progress has been made in understanding the nucleation and growth mechanism of thin films [71–73]. The structural evolution of thin film undergoes three main stages:

(i) In the early stage, vapor will condense on the substrate and migrate to a site where lowest activation energy is available for the nucleation to occur. It is called the nucleation stage (Fig. 3a).

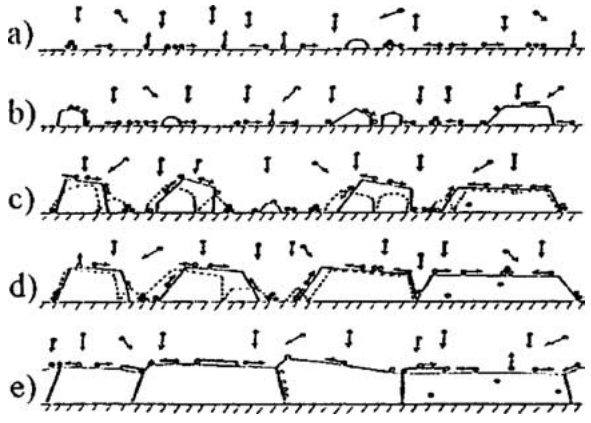

Figure 3 Schematic diagram illustrating nucleation and growth sequence of thin films [44].

(ii) Next step is the incorporation of incoming condensation flux into the growing individual units of the film structure. The condensate will try to re-structure in order to reduce surface free energy (Υ). This step is called a crystal/film growth. Since the surface free energy is generally an anisotropic property, crystal growth will take place initially in all directions to reduce the surface free energy (it will follow the stages as shown in Fig. 3b and c).

(iii) Re-organize the unit structure of the film. It is called grain growth by coalescence (as shown in Fig. 3d and e). This depends upon the substrate deposition temperature, or total energy of the system.

It is evident from Fig. 3 that the final structure of the film is a result of the creation of multiple nucleation events followed by subsequent growth of the structural units (grains in crystalline materials) and their periodic reorganization during coalescence. The continuous growth and coalescence process is associated with the surface free energy, surface diffusion and bulk diffusion that are dependent upon the substrate deposition temperature and total energy of the system. During the growth process, individual grains grow in the form of single crystals. Microstructural evolution of the thick films and bulk coatings have been investigated as a function of melting point of coating materials (T_{MP}), substrate temperature (T_{sub}), and pressure during the deposition and is summarized by the well known structure zone models as shown in Fig. 4a [74–78]. Zone 1 consists of dome topped, tapered crystals separated by voids and such microstructure is observed at homologous temperature $T_{sub}/T_{MP} < 0.3$ and is due to insufficient surface diffusion of adatoms. Transition zone or Zone T (ZT) microstructures generally occur in energy-enhanced deposition processes (i.e., IBAD and higher temperature). The additional energy increases atom mobility resulting in fewer voids between the discontinuous columns observed in Z1 microstructure. ZT structure is often densely packed fibrous grains. Zone 2 (Z2)consists of dense columnar grains with a smooth, sometimes faceted surface, resulting from surface dominant condensation and is observed at

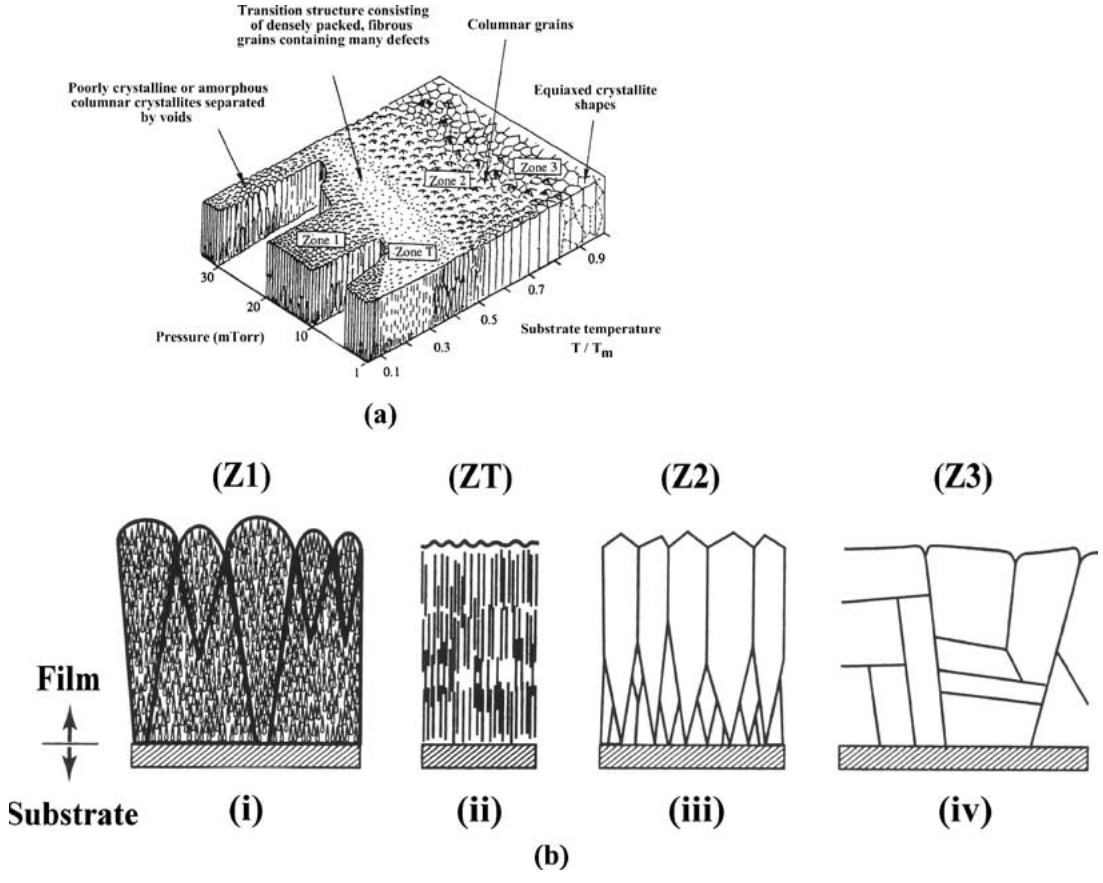

Figure 4 Schematic diagram illustrating (a) growth model with Zones 1–3 and (b) various growth morphologies in the coatings [75–79].

homologous temperature $0.3 < T_{sub}/T_{MP} < 0.5$. At very high substrate temperature (homologous temperature $0.5 < T_{sub}/T_{MP} < 1$), equiaxed grains develop from the dominance of bulk diffusion and is defined as Zone 3 (Z3).

Columnar growth structure of Zone 2 has been well investigated. Schematics of some growth structure of Zone 2 are shown in Fig. 4. Texturing of columnar grains is categorized by the kind and origin of orientation. The origin of texturing is associated with nucleation and subsequent growth. Nucleation orientation results from nucleation with the preferred plane parallel to the local substrate surface when the vapor is supersaturated and nucleation rate is high. Nucleation orientation appears only as an initial orientation. Growth orientation develops in a supersaturated region in which two dimensional nucleation on the growing crystal surface is no longer the rate-determining step. In this case, growth competition occurs between different oriented crystals. Crystals with low surface energy will dominate and continue to grow. The crystal growth direction will depend upon many functions including substrate temperature, energy, and condensation rate. Thus, the vertical growth rate is function of crystal orientation and vapor incidence angle (VIA) of the substrate.

Typically, the energy of the vapor cloud generated by thermal evaporation ranges from 0.1 to 1 eV and can be increased by interaction with higher energy ions or plasma [79]. The higher energy in the vapor cloud introduces more non-equilibrium states. The advantage of increasing the vapor cloud energy is the enhancement of its surface mobility during condensation resulting in better metallurgical bonding with the substrate, higher coating density and ability to control preferred orientation, which will be discussed in the next section. Thus by controlling various process parameters including substrate temperature during condensation, coating flux (including continuous and discontinuous), and flux energy will allow in tailoring microstructure of the coating which will offer unique physical and mechanical properties as discussed with examples below.

Although structure zone models can explain the various microstructures which occur in PVD coatings as a function of both thermal and ion induced atom movements, no account is taken of the substrate on which the deposit is formed. The influence of the substrate on coating microstructure is two-fold: the substrate crystal structure defines the growth habit of the deposit through changes in the distribution, orientation, and size of the crystallites nucleated on the growing surface, the nature of the substrate, in terms of its thermal expansion, affects the level of internal stresses in a film. This stress is compressive when $\alpha_f < \alpha_s$ and tensile when $\alpha_f > \alpha_s$, where α_f and α_s are the coefficients of thermal expansion for the film and substrate, respectively [80].

4. Applications of the EB-PVD process

Electron beam-physical vapor deposition (EB-PVD) is a derivative of the electron beam (EB) melting technique. Perhaps the most consequential growth phase in EB technology began in the early 80's and is still in

progress. This significant progress was driven by three factors: (i) greatly improved vacuum generation technology, (ii) significant advancement in computers, and (iii) availability of high quality EB-guns. Since then, EB technology has been developed for a wide range of applications including surface treatment, welding, glazing and evaporation for coatings. Incorporation of an ion source in the EB-PVD chamber with multiple ingots has increased its versatility in developing new materials with a very wide range of applications such as micro-electronics, sensors, optics, aerospace and biomedical industries. Some successful applications of the EB-PVD and ion beam-assisted EB-PVD processes are given below.

4.1. Thin films for microelectronic industry

Microelectronic industry is constantly demanding to produce defect free thin films deposited at a relatively low temperature with controlled microstructure and good metallurgical bonding with the substrate. Ion-assisted deposition can be an effective method of altering the microstructure of films including refractory materials at low substrate temperature. This can be important in electronic materials applications involving the use of refractory metals on low temperature substrates such as the metallization of active matrix liquid crystal displays (AMLCDs). In metallization applications, refractory metals are often used due to their thermal stability, chemical resistance, and electrical properties [82, 83]. One difficulty with the use of these metals is that at low processing temperatures the structure is columnar, leading to step coverage problems [84, 85]. Studies have shown that when materials are deposited under conditions of low surface mobility, the deposit formed on the step sidewalls can be considerably different from that deposited on the horizontal surface as shown in Fig. 5.

Deposition by low temperature evaporation and sputtering has been found to produce low density coatings at steps due to a misalignment of the columnar grains growing from the substrate surface with those growing from the step (Fig. 5). These regions are extremely susceptible to be attacked by wet etchants, which leads to occurrence of line breakages during interconnect patterning. If the film is deposited under conditions favoring an isotropic rather than columnar morphology this type of defect can be prevented.

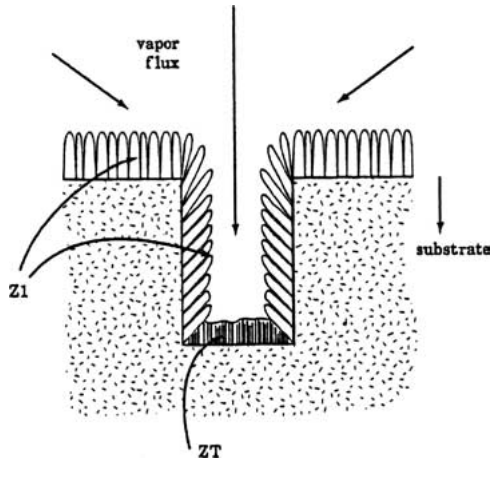

Figure 5 Schematic representation of variation in microstructure due to deposition in a trench [86].

Molybdenum films have been deposited using EB-PVD at high and low substrate temperature and with and without argon ion bombardment to determine processing conditions suitable for suppression of the columnar microstructure for fabricating films that are suitable for use as interconnects [87]. Fig. 6a–e show the interconnect lines etched from EB-PVD Mo films deposited under various processing conditions.

The stress states of these films were also investigated to determine the effect of temperature and bombardment on film stress. Of these films, the ones showing the least amount of preferential etching were those deposited under high bombardment and concurrent substrate heating as shown in Fig. 6d and e. The film evaporated with no substrate heating or bombardment is particularly poor quality due to weak adhesion of the film to the substrate (Fig. 6). It appears that bombardment or temperature alone is unable to sufficiently alter the microstructure of the Mo film as shown by Fig. 6b and c. However, the combination of the two is sufficient to suppress formation of the columnar microstructure leading to step induced defects.

Fig. 7 shows a comparison of residual stresses present in films produced by ion assisted EB-PVD and sputtering with various RF powers. Fig. 7 shows that through ion bombardment the residual stress state within the coating can be changed from highly compressive to tensile depending on the substrate temperature, energy and current density of the bombarding atoms. In summary, Mo evaporated by EB-PVD with argon ion beam assistance, resulted in the suppression of the columnar structure, better step coverage, and defect-free interconnects [87]. In addition to modifying the microstructure, the stress states of the films can be varied from tensile to compressive with ion bombardment.

4.2. Superhard coatings for machining tools and forging die industries

Metallic borides, carbides, nitrides, and oxides have been known to be very hard and wear-resistant materials. Applying these hard coatings to cutting tools and inserts can increase their life by several hundred percent (400–600%), reducing costs associated with tool procurement, set-up time, and machine down time. Wear-resistant coatings are often characterized as having high melting temperatures as well as high hardness values. Performance of the coating depends on many factors including structural, chemical and thermal stability, metallurgical bonding and machining conditions. All these factors depend upon the process selected for applying the coatings along with its microstructural characteristics including grain size, degree of texture, and density. Most wear-resistant coatings are applied by either CVD or PVD-sputtering with typical coating thickness between 2–6 μm.

The first wear resistant coatings were primarily monolithic films of transition metal- nitrides and

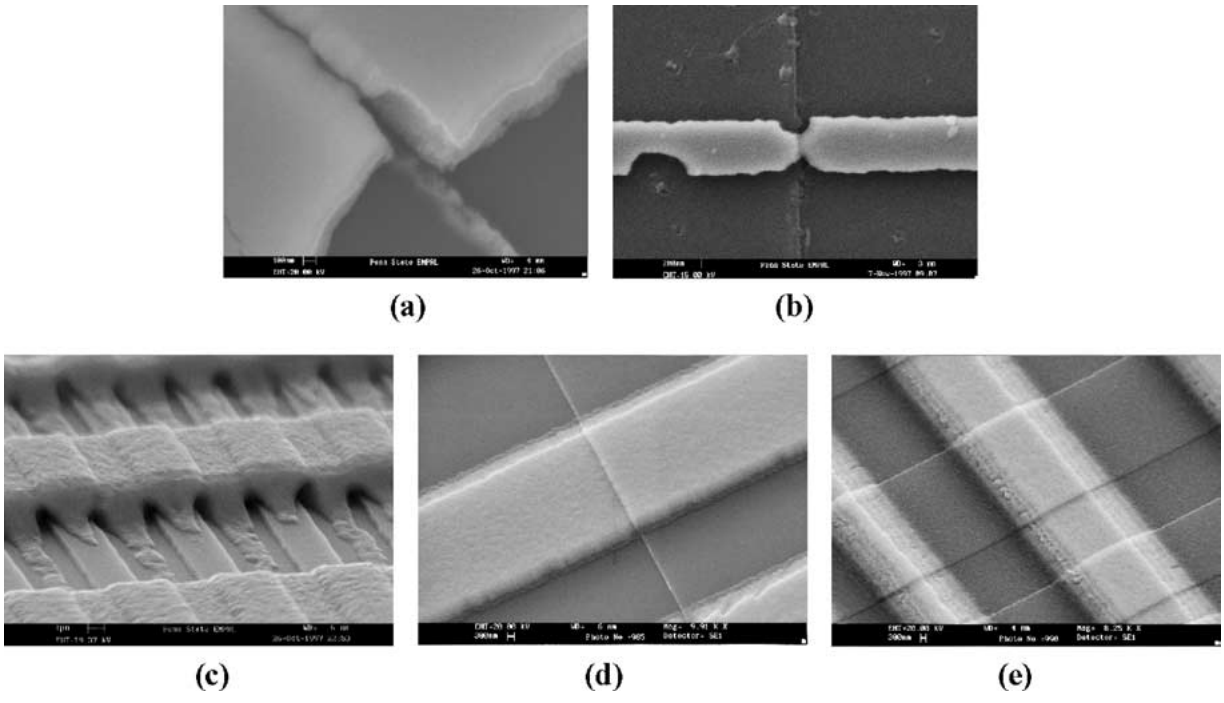

Figure 6 Molybdenum films deposited at (a) ambient temperature and no ion-assist, (b) 600°C and no ion-assist, (c) ambient temperature with ion-assist, (d) 400°C and ion-assist, and (e) 600°C with ion-assist by EB-PVD.

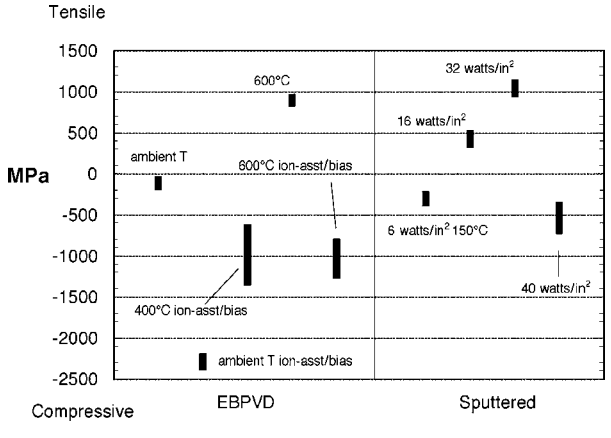

Figure 7 Stress states of EB-PVD and sputtered films [9].

carbides were commercially applied by CVD process, but today are applied by both CVD and PVD [88–95]. However, there are two main challenges in the CVD process. First, CVD is a high-temperature deposition process (>800–1200°C), and thus coating temperature-sensitive substrates is limited. Second, the environmental concern in which hazardous chemical gases are often produced during the CVD coating deposition process (details are given in the Appendix). In contrast, PVD coatings are deposited below 500°C, and are more environmentally friendly as hazardous chemical gases are not produced. In addition, PVD processes often allow coating deposition at low substrate temperatures as they do not rely on heat (temperature) for chemical reactions to take place; therefore, low melting temperature materials such as plastics can be coated. For the last few years, the trend in applying wear resistant coatings has changed from single layer to multi layers coatings (typically composed of TiN/AlN, TiN/TiC/TiN, TiN/CrN, and TiN/NbN) that offer superior performance during machining operations [96–100]. In addition, research effort is underway in different laboratories to develop new hard materials including TiBCN [101].

4.2.1. TiC by reactive ion beam assisted (RIBA), EB-PVD

In an effort to understand the effect of ion beam current density on the microstructure and hardness of TiC coatings by RIBA, EB-PVD, several samples were deposited under identical processing conditions: (T_{sub} = 650°C, constant pressure ($2–3\times10^{-4}$ torr), and gas flow ratio (1:3) of argon and C_2H_2) with the exception of the degree of ion bombardment (27–162 μA/cm^2). The hardness values ranged from 1720 $VHN_{0.050}$ to 3500 $VHN_{0.050}$ over the range of 27–162 μA/cm^2. The general trend shows that the hardness of the TiC coating increases with increasing levels of ion bombardment as shown in Fig. 8. The general accepted bulk hardness value for TiC is ~2800 VHN [29]. The TiC coating deposited with an ion beam current density of 162 μA/cm^2 (3500 $VHN_{0.050}$) showed over 25% improvement in the hardness value (near stoichiometry). It should be noted that due to the limitations of the ion source, current densities above 162 μA/cm^2 are not possible under these processing conditions.

Similarly, when the TiC coatings were deposited at constant ion beam current but in the temperature range of 250 to 750°C, the hardness values ranged from 1300 $VHN_{0.050}$ to 2270 $VHN_{0.050}$ [102]. The general trend showed that the hardness of the TiC coating increased as the process temperature was increased from 250 to 650°C. The lower hardness value at T_{sub} = 750°C is most likely a combined effect of composition, microstructure, and crystallographic texturing ⟨200⟩

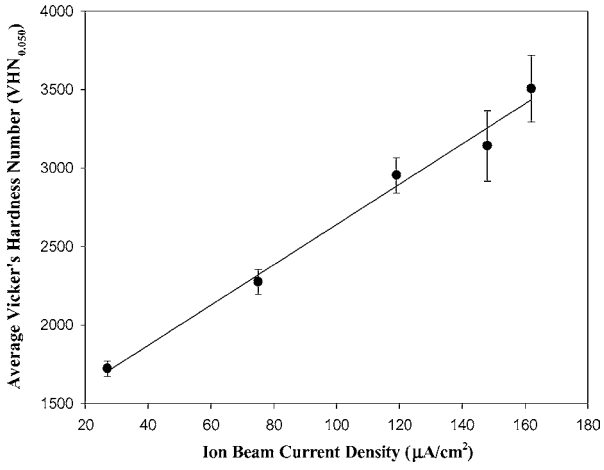

Figure 8 Average Vicker's hardness number ($VHN_{0.050}$) as a function of ion beam current density ($\mu A/cm^2$) for TiC coatings deposited by RIBA, EB-PVD at constant substrate temperature (650°C).

orientation. Variation in the hardness values is a direct result of processing temperature (ignoring variations in the deposition system), which influenced the composition and microstructure (i.e., crystallographic texture, density, surface morphology) of the TiC coatings discussed elsewhere [102].

TiB_2 coatings formation by direct evaporation

Often, direct evaporation of multicomponent materials results in fractionation. In the case of direct electron beam evaporation of TiB_2 a TiB_{2-x} coating was produced with a hardness of 2940 $VHN_{0.050}$ [28]. The hardness of the coating was increased to 3040 $VHN_{0.050}$ by argon ion beam assisted deposition. The hardness of the TiB_{2-x} coating was further increased to 3340 $VHN_{0.050}$ by applying a negative bias and bombarding the TiB_{2-x} growing film with argon ions during deposition. The resulting surface morphology shows a uniform, fine-grained surface with an average grain size of less than 100 nanometers as shown in Fig. 9. One of the main challenges in the direct evaporation of TiB_2 is the loss of B due to fractionation (dissociation of Ti and B) resulting in nonuniform-stoichiometric composition, i.e., TiB_{2-x}. The loss of boron can be compensated by introducing boron tetrachloride gas into the evaporation chamber during deposition. Unfortunately, boron tetrachloride is colorless, odorless and poisonous which causes safety issues. Instead, the TiB_2 pool was enriched with boron metal to account for the loss of B from TiB_2 fractionation.

4.2.2. TiBCN

Very limited research has been conducted in producing TiBCN by using ion beam assisted EB-PVD. This research article will demonstrate the application of EB-PVD in engineering new coating materials for cutting tool industries applied in a cost effective and environmentally friendly manner. Hard coatings such as TiN, TiC, HfC, ZrC, TiB_2 and TiBCN have been produced by ion beam-assisted EB-PVD at relatively low temperatures [28, 101–103]. Metallic-nitride coatings were produced by evaporating target materials (such as Ti, Zr, Hf) and reacted with ionized nitrogen gas resulting in nitride coatings (RIBA, EB-PVD). Metallic carbides are easy to produce by co-evaporation of two target materials: metallic (such as Ti) and graphite in the EB-PVD chamber. Graphite is difficult to evaporate as it sublimes. This challenge has been addressed by indirectly evaporating graphite using a molten pool of tungsten (W) above the graphite target material C(W) [101]. Selective results on coatings produced by reactive ion beam-assisted EB-PVD is summarized below.

A novel approach was developed in forming TiBCN in our laboratory. Three ingots Ti, TiB_2 and C(W) were co-evaporated simultaneously [101]. During the evaporation, nitrogen/argon gas mixture was introduced through the ion source. The ionized nitrogen gas was reacted with the Ti, TiB_2, and C(W) forming TiBCN super hard coatings. The loss of B was compensated by incorporating C and N into TiB_{2-x} resulting in TiBCN. The average hardness of TiBCN as function of the atomic fraction of B, C, and N is given in Fig. 10.

4.2.3. Multilayers

Fig. 11 shows the fracture surface of a TiB_{2-x}/TiC multilayer coating deposited on a WC-Co cutting tool. The TiC (grown by RIBA, EB-PVD) serves as a bond coat as well as to prevent chemical reactions between the TiB_{2-x} and substrate material. The cross section of the coatings exhibited good interface between the

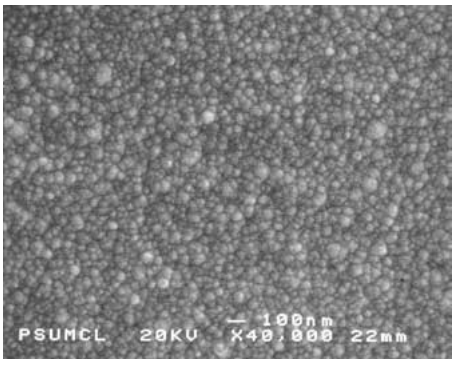

Figure 9 SEM micrographs showing nano-grained TiB_{2-x} coatings deposited on Si substrate by Sciaky EB-PVD at 750°C.

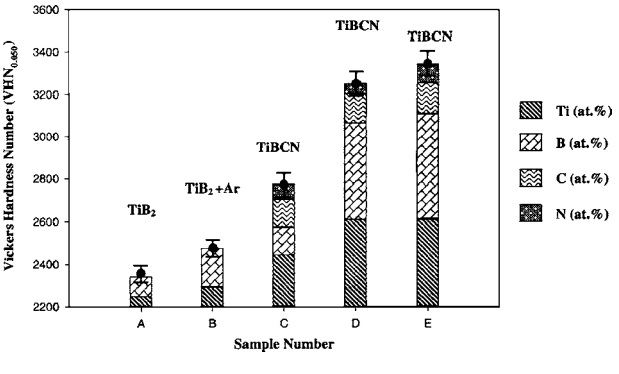

Figure 10 Average Vickers hardness number (VHN) for TiB_2 and TIBCN coatings deposited on WC-6 wt%Co-0.3 wt%TaC by argon/nitrogen ion beam assisted, co-evaporation by EB-PVD [29].

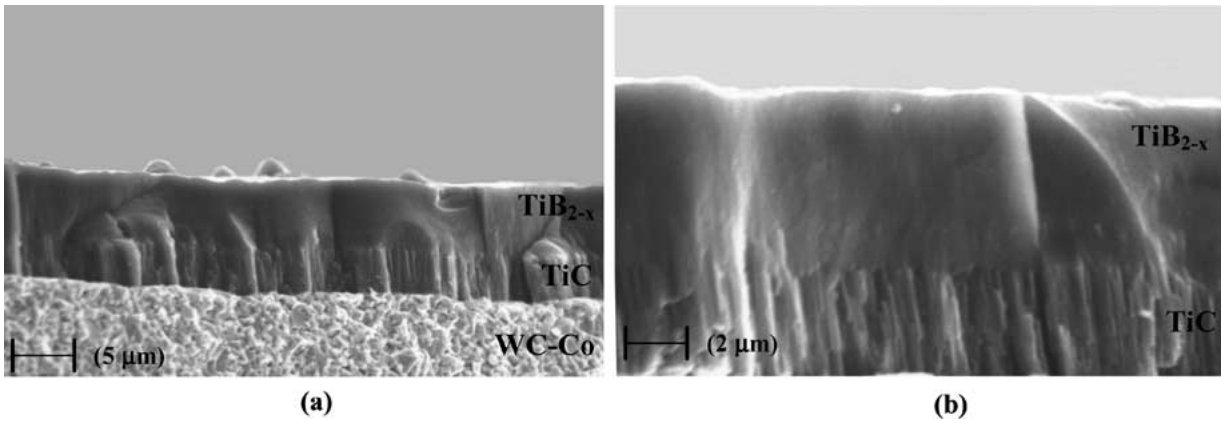

Figure 11 SEM micrograph of a fracture surface of TiB_{2-x}/TiC coating deposited on WC-Co cutting tool (substrate) showing excellent bonding interface between the coatings [29].

TiC and TiB_{2-x}. The TiC coatings exhibited columnar structure whereas the TiB_{2-x} exhibited a nano-grained microstructure. Similarly, multilayered coatings composed of TiC/Cr_3C_2 have been successfully produced by the co-evaporation of the Ti, Cr, and graphite ingots in the EB-PVD chamber as shown in Fig. 12. The thickness of each layer within the multilayer coating can be varied depending on the evaporation rate, as well as the deposition process parameters.

4.3. EB-PVD as an alternative to hard chromium electroplating

There are many auto and aerospace components coated with chromium by the electroplating process as it offers excellent surface finish, wear, erosion, corrosion and oxidation-protection (upto 600°C). However, chromium (Cr) electroplating process is well known to be an environmentally hazardous process due to generation of hexavalent chromium [105]. An environmental friendly process and material is required to replace the traditional chromium electroplating process. To achieve this goal, two challenges must be met: (1) identify potential candidate materials for the replacement of Cr and (2) develop/identify a process for applying candidate coating materials. The selection of the alternative coating processes depends upon the application and requirements including surface finish, wear-resistance properties and, fatigue and thermal properties. Three coating processes (thermal spray processes, laser cladding, and physical vapor deposition) have been considered as replacements for the electroplating process. Dini [106, 107], Oberlander and Lugscheider and Schroeder and Unger [105] have presented comprehensive reviews about various coating processes along with their shortcomings and advantages.

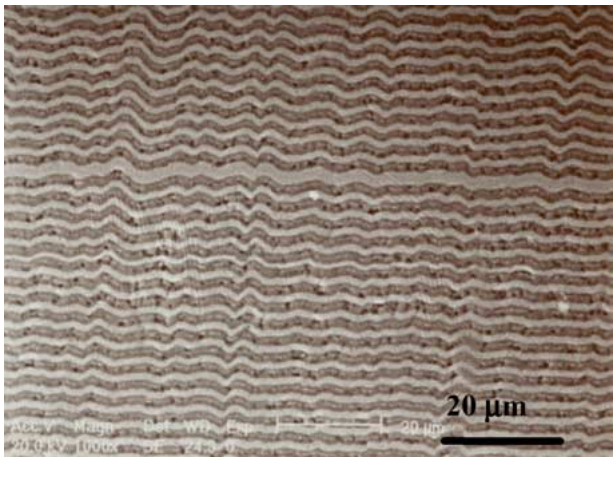

Figure 12 Optical micrograph showing multilayered TiC/Cr_3C_2 coatings produced by co-evaporation of three different ingots: Ti, Cr, C in the EB-PVD chamber [104].

Among the spray coating processes, High-Velocity Oxygen-Fuel (HVOF) has been considered as a potential candidate replacing the electroplating process. The HVOF is a cost-effective process. The WC-Co alloy has been identified as an alternative coating material replacing the hard chrome. There are mainly three shortcomings in the HVOF applied WC-Co coatings on large components such as aircraft or helicopters landing gears. First, HVOF applied WC-Co coatings have non-uniform microstructures containing un-melted powder particles and porosity (Fig. 13) [108]. Non-uniform distribution of un-melted particles and porosity in the coating limits the component life, as well as reliability. Second, it is not economical and it is difficult to repair the localized damage in WC-Co coated components. Third, the coating produced by HVOF has a rough surface which often requires additional machining steps which add costs.

A unique characteristic of EB-PVD is that it meets the above-mentioned challenges and can be used to tailor coatings for specific applications. With the ion beam assisted deposition EB-PVD process, corrosion-resistant materials can be applied economically [109]. Applications for these coatings range from brass lighting fixtures to landing gears and other components of aircrafts and helicopters. Ion beam assisted (IBA), EB-PVD process offers additional flexibility in repairing localized damage in landing gears that are temperature sensitive and require dense coatings at low substrate temperatures in order to avoid degradation of the physical and mechanical properties of the base material [105].

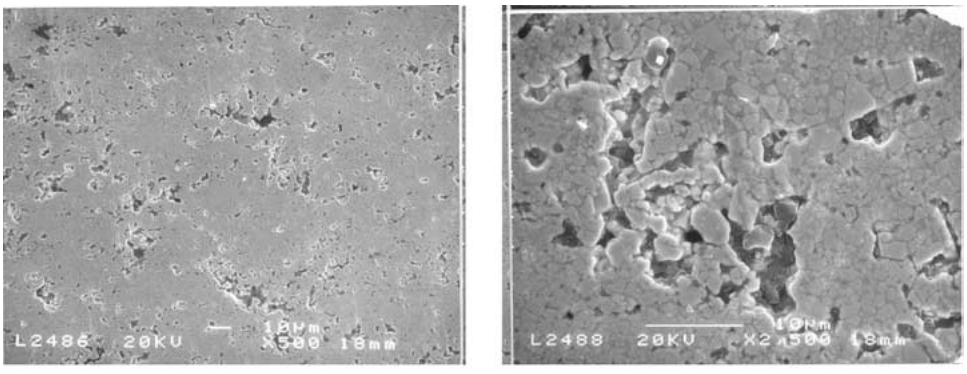

(a) (b)

Figure 13 Low (a) and high (b) magnification SEM micrographs of WC-Co coatings deposited by HVOF showing non-uniform microstructure and porosity [110].

Currently there is no localized repair process available for chromium electroplated components. The chromium coating must be stripped completely by chemical etching processes, and then recoated followed by surface machining or finishing. This research effort was undertaken to demonstrate the localized repair by ion beam assisted deposition. Fig. 14a is a photograph of a helicopter landing gear showing localized surface damage (∼0.010″) that needs to be repaired. Localized refurbishment of the landing gear (Fig. 14b) was successfully demonstrated by applying Cr in the ion beam assisted, EB-PVD chamber. The SEM micrograph of the EB-PVD Cr deposit exhibited relatively denser coating (region a of the Fig. 14b) than the electroplated Cr which contains voids between columnar grains (region b of the Fig. 14b). Unlike thermal spray coatings, these deposits had a dense microstructure with good metallurgical bonding with the base metal resulting from the IBAD process.

The significant advantage of using IBA, EB-PVD is enhancing metallurgical bonding of the coating with the substrate at a relatively low temperature. For example, EB-PVD chromium coatings flake or de-bond from the landing gear when deposited below the substrate temperature of 280°C (<550°F). This was most likely due to poor metallurgical bonding and high residual stresses in the deposit. However, when Cr was electron beam evaporated and simultaneously bombarded with ionized argon gas, the coating had a dense microstructure with good metallurgical bonding between the base material as well as the electroplated chromium (region b of Fig. 14b).

4.4. Thermal barrier coatings (TBC) for turbine industry

There is a continuous two fold thrust within the department of defense (DoD), and commercial turbine industry (including land based and aerospace) to double the thrust-to-weight ratio and extend the life and performance of turbine components under severe environmental conditions including erosion, oxidation, and corrosion. Turbine components are generally made of nickel-based super alloys. The life of turbine components is increased by applying oxidation-resistant coatings composed of platinum-aluminide (Pt-Al) or MCrAlY alloys (M = Ni, Co, Fe, or mixed combination) beneath a thermal barrier coating (TBC) composed of yttria stabilized zirconia, i.e., ZrO_2-8 wt% Y_2O_3 (8YSZ), which is an ideal candidate for thermal protection coatings because of its low density, low thermal conductivity, high melting point, good thermal shock resistance and excellent erosion resistant properties. 8YSZ has gained widespread acceptance as a TBC material for turbine applications and is generally applied by either plasma spray or EB-PVD processes [111–114]. Comparative properties of 8YSZ produced by plasma spray and EB-PVD are

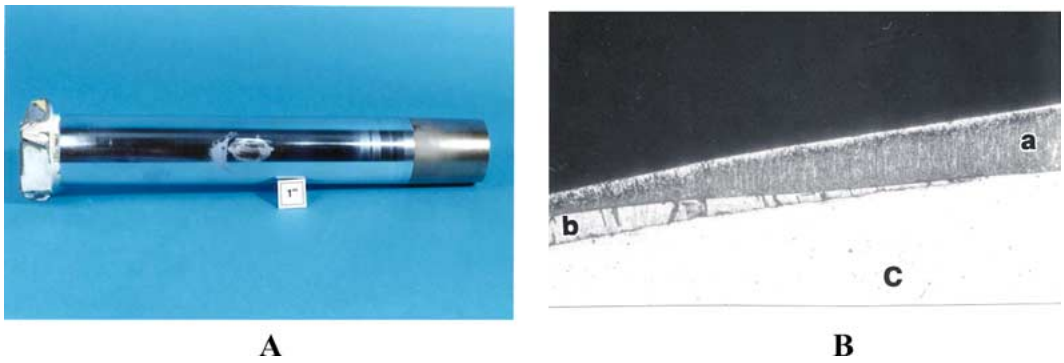

A B

Figure 14 (A) Photograph showing a helicopter landing gear with localized surface damage and (B) SEM micrograph of the refurbished region showing good metallurgical bonding of the Cr deposited by argon IBA, EB-PVD (region a) on the electroplated Cr (region b) and base material (region c) [110].

TABLE III Selective properties of TBC produced by thermally sprayed and EB-PVD processes

Properties	EB-PVD	Plasma sprayed
Thermal conductivity (W/mK)	1.5 (remains constant during thermal exposure)	0.8–>1.8 (changes during thermal exposure)
Surface roughness (μm)	1.0	10
Adhesive strength (MPa)	400	20–40
Strain tolerance	Excellent	Poor
Erosion rate (Normalized to EB-PVD)	1 (Excellent)	7 (Poor)
Microstructure	Columnar	Lamellar

given in Table III and their microstructure in Fig. 15, respectively.

TBC applied by EB-PVD process provides advantages over the plasma spray process that includes better strain tolerance, erosion-resistance, bond strength, and surface roughness despite the disadvantage of slightly higher initial thermal conductivity [115, 116]. In thermally sprayed TBC, typical grain size is approximately 1–2 μm and the coating microstructure is associated with inter-splat boundary porosity, unmelted, partially melted particles and micro-cracks [117]. In EB-PVD, TBC grain sizes vary from 1 to 2 μm near the bond coating/TBC interface, while the TBC columnar grain length is often 100–250 μm in thickness with a high degree of crystallographic texture. Keeping the total thickness of the TBC constant, the alignment of the inter-splat boundaries with typical spacing of 1 to 10 μm in the case of thermally sprayed coatings with voids, micro-cracks have a more pronounced effect on lowering the thermal conductivity than with EB-PVD. The initial thermal conductivity of thermally sprayed 8YSZ is 0.7–0.9 W/m-K which is lower than the bulk theoretical values 2.2–2.6 W/m-K [116]. However, within the first few hours of turbine engine operation, the thermal conductivity of plasma sprayed TBC can increase to 1.5 W/mK due to high temperature sintering effects.

The inter-splat/microcracks/porosity provides initial low conductivity for the plasma sprayed coatings mainly because they are involved with air gaps—air is good thermal insulator compared with zirconia (air has poor thermal conductivity), not because of the reduced mean free path for photons/phonon [116]. In addition, the splat boundaries are probably few compared to grain boundaries in producing significant phonon scattering effect. Nevertheless, the inter-splat porosity and boundaries are more effective in reducing the thermal conductivity of the material than the columnar porosity in EB-PVD coatings because of the increased thermal resistance and phonon scattering in the heat conduction direction. If, heat resistance and greater phonon scattering associated with the plasma sprayed TBC microstructure could be applied to TBC produced by EB-PVD, it could make a significant contribution to the reduction of the thermal conductivity. In addition, radiative heat transport becomes increasingly important at high temperatures, so producing a TBC microstructure that also increases infrared (IR) photon scattering will help decrease heat transport through the TBC at high temperatures. Thus, a modified microstructure of the EB-PVD TBC appears to be very promising method in lowering the thermal conductivity of the coating. Very limited research has been conducted in this area which could significantly impact the turbine industry by producing TBC materials with lower thermal conductivity for high temperature applications. It is important to distinguish the effects of phonon scattering, which decreases thermal conductivity, and photon scattering which reduces radiative heat transport. Both scattering properties are influenced by the presence of interfaces including voids, micro-porosity and grain boundaries; however, phonon scattering is effected by smaller dimension features than IR photon scattering.

The typical microstructure of a TBC produced by EB-PVD can be divided into two zones (Fig. 16a). The inner zone (I) is the early part of multiple nucleation and subsequent growth of the columnar microstructure having large number of interfaces, grain boundaries, microporosity and randomly oriented grains. The thickness of the inner zone ranges from 5 to 10 μm that exhibits lower thermal conductivity (around 1.0 K/mK). With increasing thickness, the structure is characterized by a high-aspect ratio columnar grain structure with dominant crystallographic texture. The thermal conductivity increases as the outer part of the coating behaves more like a single crystal (zone II). In this outer zone (II), the

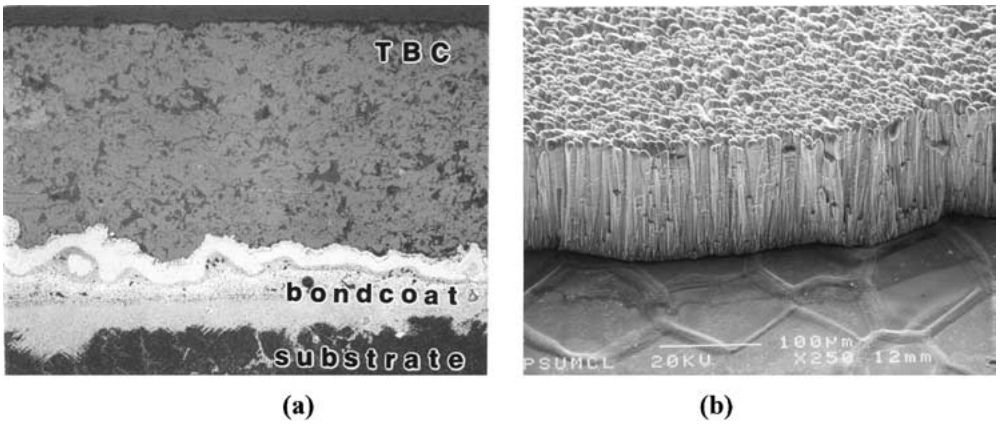

Figure 15 (a) Optical micrograph of plasma sprayed TBC and (b) SEM micrograph of the fractured EB-PVD-TBC showing columnar grains [10].

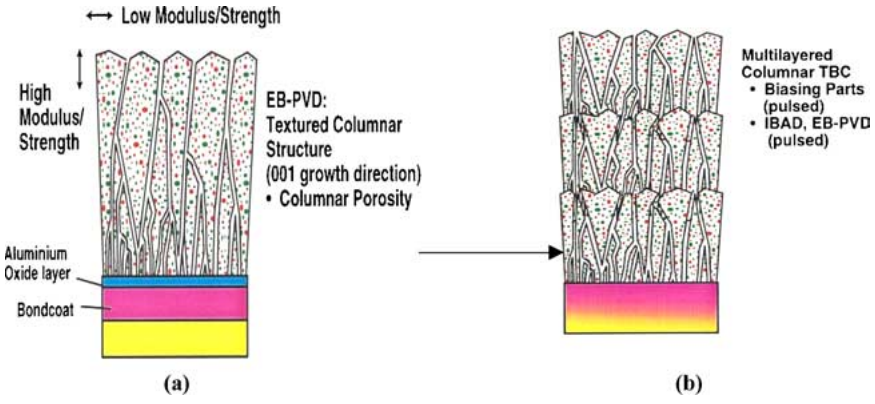

Figure 16 Schematic diagram showing: (a) a typical standard vapor phase columnar microstructure and (b) modified columnar microstructure with multiple interfaces [10].

thermal conductivity approaches that of bulk zirconia (2.2 W/mK). Thus, modifying TBC structures should offer the best properties available for commercial EB-PVD coatings: namely, low thermal conductivity, high strain tolerance, and good erosion resistance. Combination of layering at the micron level and introduction of density changes from layer to layer will significantly reduce the thermal conductivity of the coating (Fig. 16b). As mentioned earlier, layered periodicity in the coating will significantly reduce both phonon scattering and photon transport.

A microstructure similar to Fig. 16b, i.e., periodic interfaces and microporosity in the TBC was produced by two approaches. The first approach used was to periodically interrupt the continuous vapor flux by translating the sample away from the vapor cloud for a short period (30–60 s) and then re-introducing the samples into the vapor cloud. During this interruption, the temperature of the sample decreased from ∼1000 to ∼750°C. Due to the combination of discontinuous condensation and thermal fluctuations of the sample's surface temperature during this "in and out" method, new grain formation occurs (similar concept as with inter-splat boundaries in plasma sprayed TBC). It was theorized that during nucleation and subsequent growth of the first TBC layer on the polycrystalline PtAl coated substrate, the TBC would exhibit randomly oriented grains (i.e., similar to zone I of Fig. 16a, which generally occurs during standard single layer 8YSZ deposition). After the interruption, the subsequent nucleation of the second layer (on the previous grown textured layer (zone II)) will again exhibit crystallographic texturing similar to zone I resulting in relatively more random texturing. As additional material deposits on the sample, the grains grow with the zone II structure and crystallographic texture. After each interruption, sharp interfaces between the new grains and the previously formed grains are observed as shown in Fig. 17. Due to the faceted surface morphology of columnar grains, additional microporosity develops at or near each interface of the next nucleating TBC layer. The interfacial volume fraction of the distinct interfaces and degree of micro-porosity depends on the periodicity or total number of layers. This concept is referred to as the "in & out" approach as shown in Figs 16b and 17. By increasing the total number of layers, the volume fraction of randomly oriented grains (near zone I of each layer) increases and as anticipated, it was found to be less crystallographically textured when compared to a standard single-layered TBC. This was confirmed by X-ray diffraction patterns as shown in Fig. 18. In general, a standard single layered 8YSZ coating shows a strong ⟨200⟩ crystallographic texture. Although the layered TBC (Fig. 18b) shows a ⟨200⟩ crystallographic orientation, the observance of additional high index planes in the TBC could be due to many factors including high volume fraction of multiple nucleation and growth of grains (interfaces) [118]. The subsequent growth of these grains during deposition will change its crystallographic growth orientation. The change in grain orientation is believed to be the

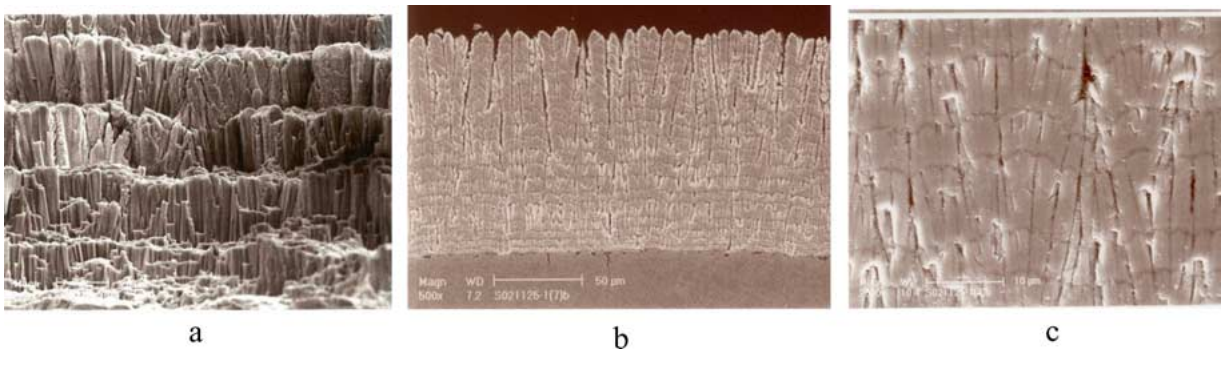

Figure 17 SEM micrographs showing: (a) fractured surface, polished surface at (b) low magnification and (c) high magnification of 8YSZ produced by EB-PVD using "in & out" method exhibiting multiple sharp interfaces.

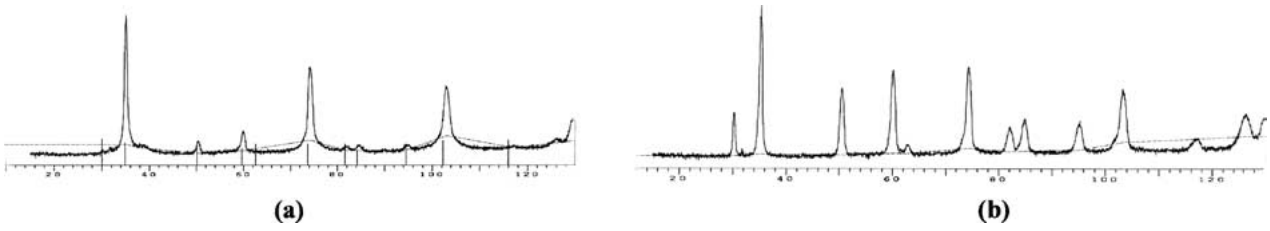

Figure 18 X-ray diffraction pattern of (a) single layer and (b) 20 layers of TBC produced by EB-PVD.

result of competition between strain energy and surface free energy.

The second approach used was to periodically interrupt the continuous flux of the vapor cloud by using a "shutter" mechanism. It is important to mention here that the temperature of the substrate remained constant during the deposition process (whereas it decreased to ∼750°C during the "in and out" method"), but discontinuous vapor condensation still occurred. During this interruption period, it is believed that the surface mobility of the condensed species contributed towards surface relaxation. As the vapor flux is prevented from condensing on the surface, the surface atoms with high surface energy and mobility have more time to diffuse to regions of lower surface energy. The periodic relaxation and deposition will contribute in forming layered materials with localized compositional fluctuations having different elastic strains, refractive index and defect density. Viewing from the top surface of the coating, the grain size does not change, but the intracolumnar microstructure (i.e., microporosity and morphology) is believed to be altered as shown in Fig. 19a and b. Microporosity was not detected by SEM. However, microporosity was confirmed by the lower thermal conductivity values as porosity is directly related to the thermal conductivity. Since there is no temperature change, and just a disruption of the vapor flux for a short period of time, the long high aspect ratio columnar grains continue to grow to the total length of the coating thickness similar to standard single layer 8YSZ. The growth orientation of the new flux remains the same as the underlying grain, and maintains the same crystallographic texturing throughout layering of TBC produced by shutter approach (Fig. 19). Since, there is no sharp distinct interface between the condensed flux and the newly arrived flux, i.e., diffused interface, it implies that the diffused interface may contain microporosity. Periodicity of such microstructural modifications will have an impact on the thermal conductivity and thermal reflectance. This theory was confirmed by measuring the thermal conductivity and hemispherical reflectance of the layered TBC deposited by both approaches as discussed below.

Fig. 20a shows comparative thermal conductivity values of a standard single layered 8YSZ, layered TBC with diffuse interfaces produced by "shutter" method, and layered TBC with sharp interface produced by "in & out" concept. The total thickness of each coating was approximately the same. The thermal conductivity of the 10-layered TBC (shutter) is comparable with the 10-layered TBC produced by "in & out". In order to establish a relationship between the thermal conductivity as a function of total number of TBC layers, additional TBC coated samples were produced using the shutter concept. It was established that the thermal conductivity decreased linearly as a function of increasing number of TBC layers as shown in Fig. 20b. This confirms the theory that periodic interruption of the incoming flux by "shutter" method results in lower thermal conductivity as compared to a standard 8YSZ [118].

In addition to decreasing thermal conductivity, the diffuse interfaces with micro-porosity should also affect the hemispherical reflectance of the coating and therefore reduce radiative heat transport through the TBC. As shown in Fig. 21, reflectance of the coating increases as a function of the total number of layers at 1 μm wavelength, the wavelength of most interest for TBC. The reflectance was increased from approximately 35% (1-layer) to 45% (20-layers) at 1 μm wavelength. This suggests that more heat will be reflected from the coatings as the number of layers increases within the TBC. It has been found that there is an additional benefit of interrupting coating deposition by the shutter method. The TBC with diffused layers offered more strain tolerance as compared with the single layer [119]. In addition, thermal cyclic data clearly

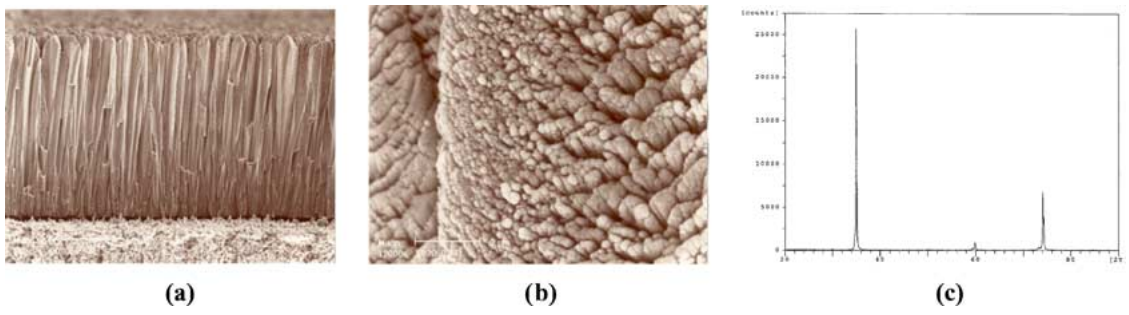

Figure 19 SEM micrographs showing a fracture surface of 8YSZ deposited by EB-PVD having 40-layers using the "shutter" method at (a) low magnification, (b) high magnification, and (c) X-ray diffraction pattern showing texturing along ⟨200⟩.

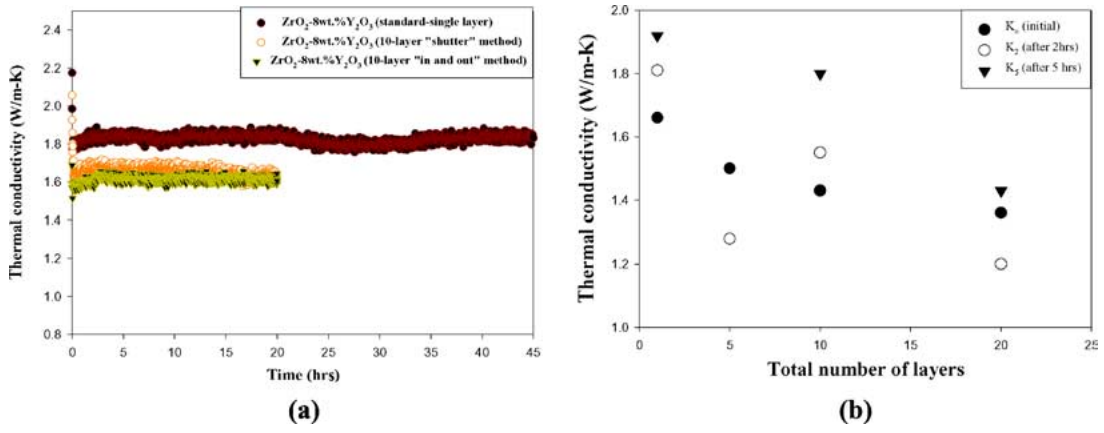

Figure 20 Thermal conductivity of EB-PVD 8YSZ coatings determined by a steady state laser heat flux technique at 1316°C: (a) thermal conductivity as a function of testing time for coatings produced by: standard continuous evaporation, flux interruption by "shutter," and flux interruption by "in & out" concept and (b) thermal conductivity of EB-PVD 8YSZ coatings as a function of total number of layers produced by the "shutter" method measured at various stages of testing, k_0-as deposited, k_2 after 2 h testing and k_5 after 5 h testing.

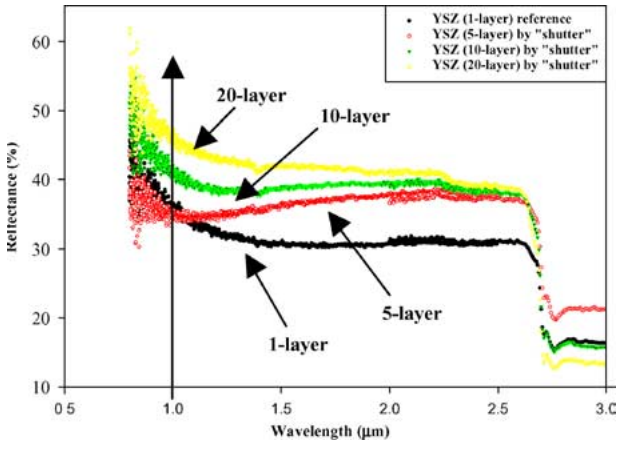

Figure 21 Hemispherical reflectance of layered (1, 5, 10, and 20 total layers) 8YSZ produced by "shutter" method after thermal exposure at 950°C for 20 h.

shows that the life of TBC coated buttons increased with increasing number of diffuse layers, with the 20-layer coating showing a 185% improvement (Table IV). Thus, overall benefit of the TBC produced by shutter method is three-fold: lower thermal conductivity (25–30%), enhanced thermal reflectance (15–20%) and enhanced strain tolerance with improved thermal cyclic life (180%) depending upon the layer periodicity [113–118].

Reflectance of the layered TBC produced by "in & out" was increased from ∼40 to 55% as the total number of sharp interfaces increased from 10 to 40 at 1 μm wavelength. However, the layered TBC prematurely failed and exhibited limited thermal cyclic life due to the presence of sharp interfaces which introduced more residual stresses.

TABLE IV Thermal cyclic data of TBC coated buttons with thermal exposure at 1175°C for 60 min and fan air cooled at RT for 10 min. TBC was applied on Pt-Al bond coated MRM 247 buttons (diameter 1″ and thickness 0.25″)

TBC deposition vendor	# of layers by shutter	Improvement
OEM	1	X-base line
PSU	1	27%
PSU	5	31%
PSU	10	125%
PSU	20	186%

The future thrust of NASA and the aerospace industry is doubling the thrust-to-weight ratio by operating engine at much higher temperature >3000°F (1648°C). 8YSZ is suitable for engine operating temperatures only up to 2200°F (∼1200°C). Therefore, there is a need in identifying a new TBC material that should be stable for higher engine operating temperatures and offer similar properties as 8YSZ, i.e., low thermal conductivity, good modulus, strain tolerance, and excellent erosion resistance properties. In the search of new TBC materials, HfO_2-based oxide materials appeare to offer desirable properties with some penalty, i.e., it is a high density material as compared with 8YSZ [119]. It is important to mention here that as the thermal conductivity of the ceramic material decreases, it becomes more difficult to evaporate as unstable melt pool and severe spitting occurs.

Two HfO_2-based materials were identified for high temperature turbine applications: HfO_2-27 wt%Y_2O_3 and HfO_2-40 wt%ZrO_2-20 wt%Y_2O_3. The thermal conductivity of two HfO_2-based alloys is shown in Fig. 22a. HfO_2-27 wt%Y_2O_3 exhibited lower thermal conductivity by 33% as compared to standard 8YSZ. The thermal conductivity of HfO_2-27 wt% Y_2O_3 was further reduced by 33% using the same concept as applied for 8YSZ, i.e., deposition coating by interrupting with shutter (Fig. 22b). Similarly, higher hemispherical reflectance of the HfO_2-27 wt% Y_2O_3 was observed as a function of number of layers produced by shutter (Fig. 23). Thus, coating interruption concept has opened an opportunity in engineering TBC materials with the desired higher reflectance and lower thermal conductive properties through micro-structural modifications and without changing composition.

4.5. High reflective thermal barrier coatings

In order to obtain a high value of reflectance in the multilayer coatings, a stack of alternate layer of high refractive index and low refractive index materials is used. Typical refractive index (n) of ceramic TBC

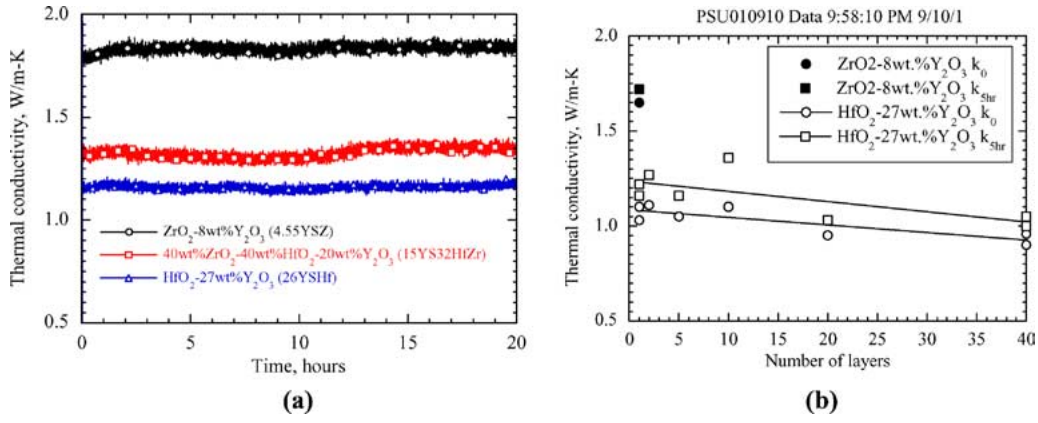

Figure 22 (a) Comparative thermal conductivity of EB-PVD 8YSZ, HfO_2-40 wt%ZrO_2-20 wt% Y_2O_3 and HfO_2-27 wt%Y_2O_3 coatings as a function of test time and (b) thermal conductivity of EB-PVD HfO_2-27 wt%Y_2O_3 coatings as a function of number of layers produced by the "shutter" method.

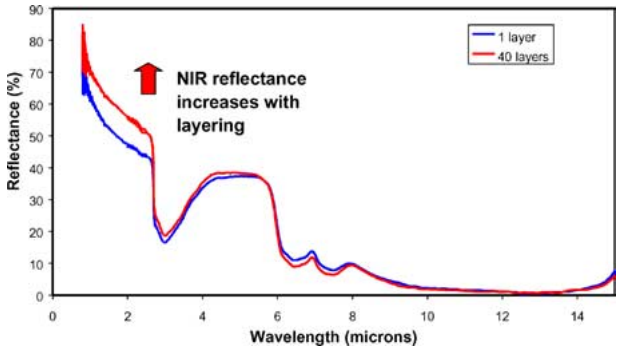

Figure 23 Hemispherical reflectance of HfO_2-27 wt%Y_2O_3 deposited on PtAl bond coated Rene N5 showing layered (shutter) vs. un-layered after 20 h @ 950°C.

materials are: ZrO_2 (2.10), CeO_2 (2.35), HfO_2 (1.98), Al_2O_3 (1.60), SiO_2 (1.95), and Y_2O_3 (1.82). Similarly, refractive index of monolithic materials can be changed by forming alternate layers of high and low density structures, i.e., modulated microstructure with density variation. Advantage of inhomogeneous antireflection coatings is that they are not sensitive to the angle of incidence. By controlling the thickness of each layer, reflectance of the coating can be controlled over a wide wavelength range. This concept was demonstrated using two materials of different composition and refractive index as described below.

Multilayer coatings were formed by co-evaporation of two materials (8YSZ and Al_2O_3) in the EB-PVD chamber as shown in Fig. 24. During co-evaporation, a partitioning was created between the two ingots to avoid any inter mixing of the vapor cloud. The mandrel on which the sample was mounted was rotated above the partitioning. The rotation speed and evaporation rate of each ingot was controlled to get the desired thickness of each layer. The thickness of each Al_2O_3 layer was varied from ~75 to 100 nm (black color) while the thickness of 8YSZ remained constant at 400 nm (white color) as shown Fig. 24. The corresponding hemispherical reflectance of the coating is displayed in Fig. 25. The reflectance of the coating varied from 75 to 50% over the wavelength of interest. This preliminary experiment clearly showed that the reflectance of the coatings can be tailored to achieve high reflectance over a wide wavelength range by controlling (altering) the thickness of each Al_2O_3 and 8YSZ layer.

4.6. Functionally graded materials

Functional graded (FG) structural materials are gaining importance in the field of high temperature

Figure 24 SEM photographs showing nanolayered 8YSZ (white color) and Al_2O_3 (black color) coatings produced by co-evaporation of two ingots: 8YSZ and Al_2O_3 in the EB-PVD chamber.

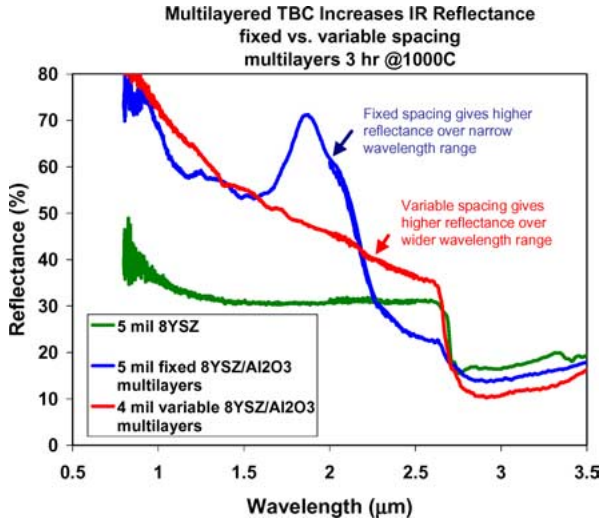

Figure 25 Hemispherical reflectance of nanolayered coatings composed of 8YSZ/Al_2O_3 produced by co-evaporation of two ingots simultaneously in the EB-PVD chamber.

applications where coefficient of thermal expansion (CTE) between different materials is one of the largest concerns. Application of FG structural materials is unlimited ranging from NASA's space rocket engines, nuclear propulsion systems, high temperature radiators, to X-ray targets. Selection of materials for forming FG structural materials is based upon the application [120–124]. NASA's space rocket engine is generally made of copper based alloys (Cu-5%Ag-0.5%Zr or Cu-8%Cr-4%Nb) which offer excellent high temperature thermal conductivity and mechanical properties for such applications [119]. The typical space rocket engine configuration is shown in Fig. 26 consisting of many cooling channels through which liquid hydrogen or oxygen is passed, maintaining the temperature well below 178 K. In the interior section of the rocket engine, the environment is extreme where liquid fuel, i.e., hydrogen and oxygen combine in the combustion zone resulting in very intense heat with temperatures reaching 800–900°C. The combustion chamber liner often degrades due to oxidation of copper, and thus need environmental protection coatings. It has been considered in applying ceramic thermal protection coatings (such as 8YSZ) on the interior of combustion chamber liner to minimize heat transfer to the copper liner without degrading its thermal conducting properties. One approach which is being considered is to apply a thin metallic coating-as a bond coat such as MCrAlY (where M = Ni, Fe, Co, or mixed combination) on the Cu-liner before applying 8YSZ. The MCrAlY material was selected as it offers excellent metallurgical bonding between the MCrAlY and ZrO_2-8 wt%Y_2O_3 and also acts as a diffusion barrier for protecting copper from oxygen. The biggest challenge is in having a minimum CTE mismatch between Cu, MCrAlY, and 8YSZ without having a sharp interface (Table V), which can only be achieved by forming a functional graded coating with a smooth compositional transition from Cu → MCrAlY → ZrO_2-8 wt%Y_2O_3. Proof of concept was demonstrated between MCrAlY and YSZ as shown in Fig. 27 formed by EB-PVD through co-evaporation of MCrAlY and YSZ. The functional graded structure was formed between the MCrAlY and ZrO_2-8 wt%Y_2O_3 in which

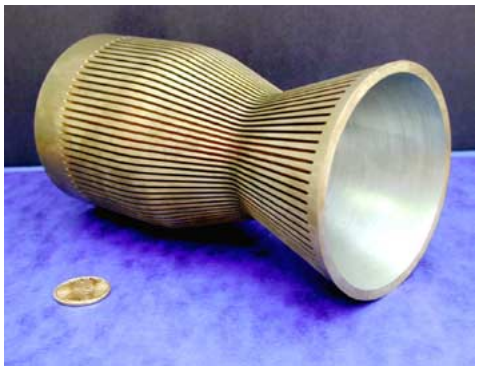

Figure 26 NASA's main combustion chamber made of copper based alloys with cooling channels.

TABLE V Coefficient of thermal expansion (CTE) of materials

Materials	Cu	MCrAlY	ZrO_2-8 wt%Y_2O_3
CTE ($\times 10^{-6}$ K^{-1})	17	15	8.9–10.6

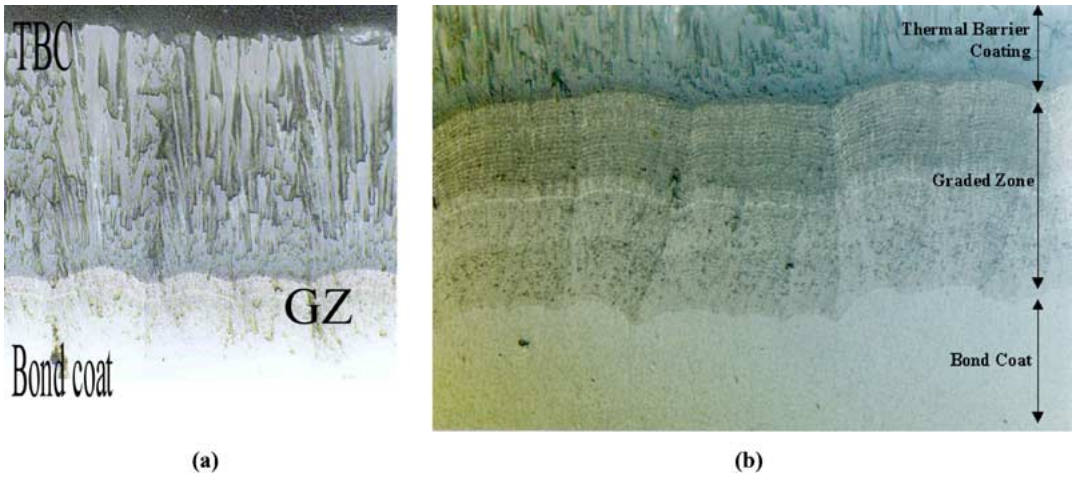

Figure 27 Cross-sectional optical micrographs (a-low magnification, b-high magnification) showing the microstructure of bond coat (i.e., MCrAlY), graded zone (GZ) and ceramic coatings (ZrO_2-8 wt%Y_2O_3) produced by EB-PVD.

during the co-evaporation period, the evaporation rate of MCrAlY was decreased and evaporation rate of ZrO_2-8 wt%Y_2O_3 was increased resulting in FG zone (Fig. 27). The deposition was continued with only YSZ being evaporated to form a top layer composed only of the ceramic coating, i.e., ZrO_2-8 wt%Y_2O_3. Future efforts would entail applying a layer of copper coating followed by co-evaporation of copper and MCrAlY on the combustion chamber liner to achieve good metallurgical bonding with the base material.

4.6.1. Functional graded Re → ReHf → Hf → HfN and Re → ReZr → Zr → ZrN coatings

A similar research effort was undertaken in applying HfN and ZrN coatings as a diffusion barrier on Re-Mo based alloy substrate for high temperature applications. One such application is for light-weight heat pipe cooled leading edges with high heat flux capabilities, where refractory-metal tubes embedded in the refractory-composite structure serve as the containers for liquid-metal heat pipe for space application [125]. Refractory metals are utilized since they exhibit high melting points and high strengths at elevated temperatures. They can also withstand high processing temperatures required for manufacturing refractory-composite materials. One of the complications encountered with embedding a refractory-metal tube in a refractory-composite structure is lack of chemical compatibility between the two materials. Many refractory metals form carbides or silicides when in contact with carbon or silicon at elevated temperatures. The formation of carbide and silicides can lower the strength and ductility of the refractory metals. In addition, for heat pipe applications, carbon or silicon may diffuse through the metal tube (i.e., heat-pipe container) and contaminate the heat pipe. In order to minimize chemical interaction between the refractory-metal heat pipe tube and refractory-composite structure, various barrier coatings are being considered. One of the diffusion barrier coatings identified is HfN and ZrN. The biggest challenge was to minimize delamination of the coating during thermal cyclic exposure caused by large CTE mismatch and poor interfaces. Functionally graded Re → ReHf → Hf → HfN structure was made by ion beam assisted EB-PVD as shown in Fig. 28. Here, Re was evaporated first followed by the co-evaporation of Re and Hf. Concentration of Hf was continuously increased and Re was decreased as a function of deposition time and coating build-up, resulting in the last layer enriched in Hf (100%). This Hf layer was then reacted with ionized nitrogen gas during deposition process forming HfN. There is no distinct interface between the Hf and the HfN structure. Fig. 28a shows the top view of the HfN coating exhibiting nano-grained microstructure. Fig. 28b shows the cross section of the functional graded coatings (Re → ReHf → Hf → HfN). It is unclear the cause of variation in the cross section microstructure of the functional graded coating in spite of continuous evaporation of Re → Hf materials without interruption.

4.7. Precision net-shaped forming components

Refractory metals are very attractive materials for high temperature structural and energy system applications such as solar powered rocket engines, heat exchangers, space and missile propulsion systems. However, it is very difficult to produce precision net-shaped components made of refractory metals such as tungsten, hafnium and rhenium with a density >95%. Typically, components are fabricated by either powder metallurgy (P/M) or chemical vapor deposition (CVD). Due to difficulties encountered in the P/M fabrication and shaping of refractory parts, CVD is mainly used in fabricating thin walled, small diameter or complex shaped components and also for coatings on carbon, ceramic and metal components. However, the CVD process also has many shortcomings. For instance, rhenium deposition is obtained by passing chlorine gas through a heated

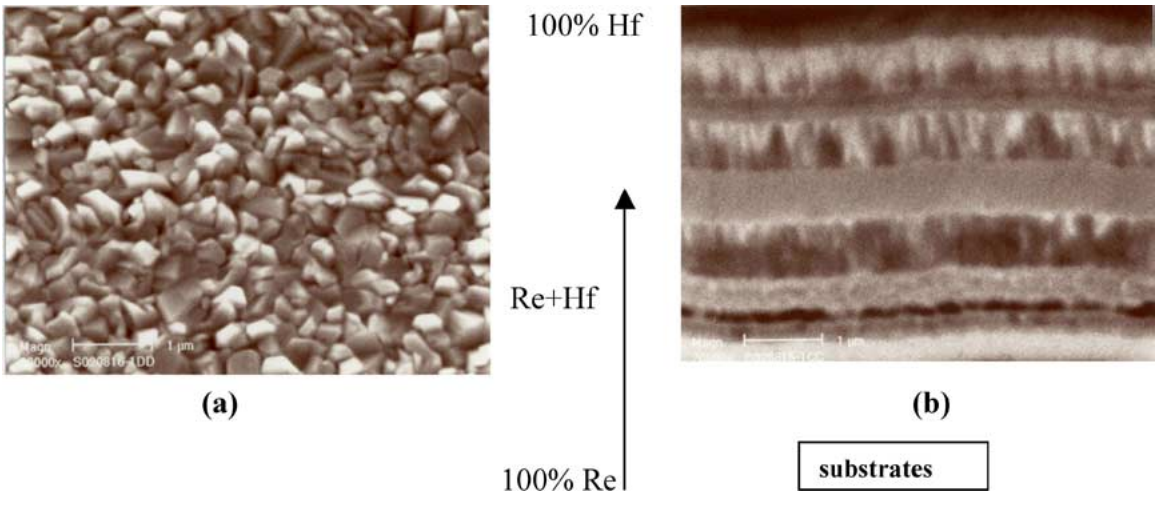

Figure 28 (a) SEM showing the top view of the coating exhibiting nano-grained microstructure, (b) cross-section scanning electron micrograph (SEM) shows a functionally graded Re → ReHf → Hf material deposited on Re-Mo alloy plate by EB-PVD [126].

chamber (at 500°C) containing rhenium chips resulting in rhenium penta-chloride ($ReCl_5$). The gaseous molecules of $ReCl_5$ decompose at 1200°C with rhenium atoms depositing on the substrate. However, CVD rhenium deposits contain entrapped gases (chlorine and hydrogen) as impurities resulting in lower physical and mechanical properties. CVD coating often produces columnar microstructure that is undesirable for structural applications. The columnar microstructure is destroyed by periodically removing partially coated components followed by mechanical grinding, i.e., partially removing rhenium coating material and continue recoating. This effort is repeated many times to obtain the desired thickness and density of the coating. It has been reported that the CVD rhenium substrate produced in this way exhibits multiple layers. When the CVD-Re component is heated to elevated temperature, individual layers tend to separate, allowing slippage. This phenomenon has shown to decrease the mechanical properties of CVD-Re, which is highly undesirable for the design and incorporation of flight engines [127, 128]. The second shortcoming of the CVD process is that it requires long fabrication time in producing components, and thus it is not a cost effective manufacturing process.

Since CVD is not a line-of-sight process, the interior and exterior of complex components can be coated simultaneously. However, it is difficult to apply uniform coating 'thickness' on spherical components, i.e., graphite balls due to limited flexibility in maneuvering parts in the reaction chamber, gas flow dynamics and entire surface area to be coated simultaneously (i.e., 360°). Depending on the dimension of the components, generally one component (such as thruster) is manufactured at a time in the CVD reactor chamber.

Powder metallurgy (P/M) techniques have been explored in the fabrication of rhenium components [129]. These techniques also have their limitations with respect to cost, speed, achievable geometry, required tooling and high temperature isostatic pressure (HIP) treatment for compaction [130]. Various steps are involved in the manufacturing of components including cold isostatic pressing, pre-sintering at 1200°C and hot sintering at 2500°C. Densities greater than 99% are achievable only after extensive amounts of accumulated cold and hot working. Hot working of rhenium must be carried out in a hydrogen environment. In air, the rhenium metal readily oxidizes to the heptoxide (melting point 297°C), so hot working in air is not possible. This extensive value-added processing contributes to high cost and fairly limited range of commercial shape components [131]. Fabrication of components by powder-plasma spray process has also been explored and exhibits poor mechanical properties due to presence of large volume fraction of porosity.

An effort was undertaken to address shortcomings of CVD and P/M techniques and identify an alternative manufacturing method in fabricating net shaped components with density >95% in a cost effective manner. Electron beam-physical vapor deposition (EB-PVD) method has met these challenges.

4.7.1. Fabrication of rhenium plate

Effort was first undertaken to demonstrate that rhenium plates produced by EB-PVD had equivalent or better physical and mechanical properties in comparison with conventional CVD process. Rhenium ingot was used as a source material that was supplied by Rhenium Alloys Inc. (density 98% and purity 99.99%). A focused high-energy electron beam was used to evaporate the rhenium ingot in the coating chamber and deposited on graphite plates. During deposition process, the graphite plates were indirectly heated up to 1000°C. The microstructure of the coating was tailored by changing various process parameters including evaporation rate, periodically interrupting incoming vapor flux, and vapor incidence angle (VIA) as shown in Fig. 29, respectively [131, 132]. A novel concept was developed to avoid any continuous columnar grain formation during deposition, i.e., used the in & out approach in forming textured subgrain microstructure as shown in Fig. 29b. In addition, rhenium plate exhibited textured grain growth with micron and sub-micron sized microstructure. Coated plates exhibited higher hardness (283VHN) in comparison with CVD rhenium plate with hardness of 245VHN. Using the Hall-Petch equation along with the grain size and hardness, it is predicted that the Re-plate will exhibit 30% improvement in mechanical properties as compared with CVD Re-plate, which was confirmed by measuring mechanical properties (tensile strength of EB-PVD Re was ~72 ksi and CVD Re was ~50 ksi). Rhenium plates were found to be free from impurities such as copper or other materials. During the course of this investigation, it was demonstrated that the growth orientation of the coatings can be changed by periodically changing the vapor incidence angle (VIA) of the incoming flux as shown in Fig. 29c.

4.7.2. Fabrication of rhenium coated graphite balls

Applying uniform rhenium coating on graphite balls (or cores) by EB-PVD is a demonstration in net-shape forming components. 17 graphite cores (diameter ~15 mm) were simultaneously charged into a cylindrical cage as shown in Fig. 30a. The cage was fabricated using molybdenum wire mesh. The cylindrical cage was rotated at 7–10 rpm above the melt pool within the rhenium vapor. During the deposition process, cores were heated to 1000°C by radiation heating under the A-frame graphite heater. The Re-coated graphite cores were also simultaneously bombarded with ionized argon gas during deposition to obtain a dense uniform microstructure. After applying rhenium to the full coating thickness, seventeen coated cores were simultaneously polished in the laboratory vibromet-polishing unit to the surface finish <Ra8 (Fig. 30b). All coated cores exhibited uniform coatings with 100% concentricity, which was measured by co-ordinate measuring machine (CMC). It is important to mention here that there are more than 250 micron and sub-micron grains through the coating thickness (2000 μm) with a much finer grain structure (Fig. 31).

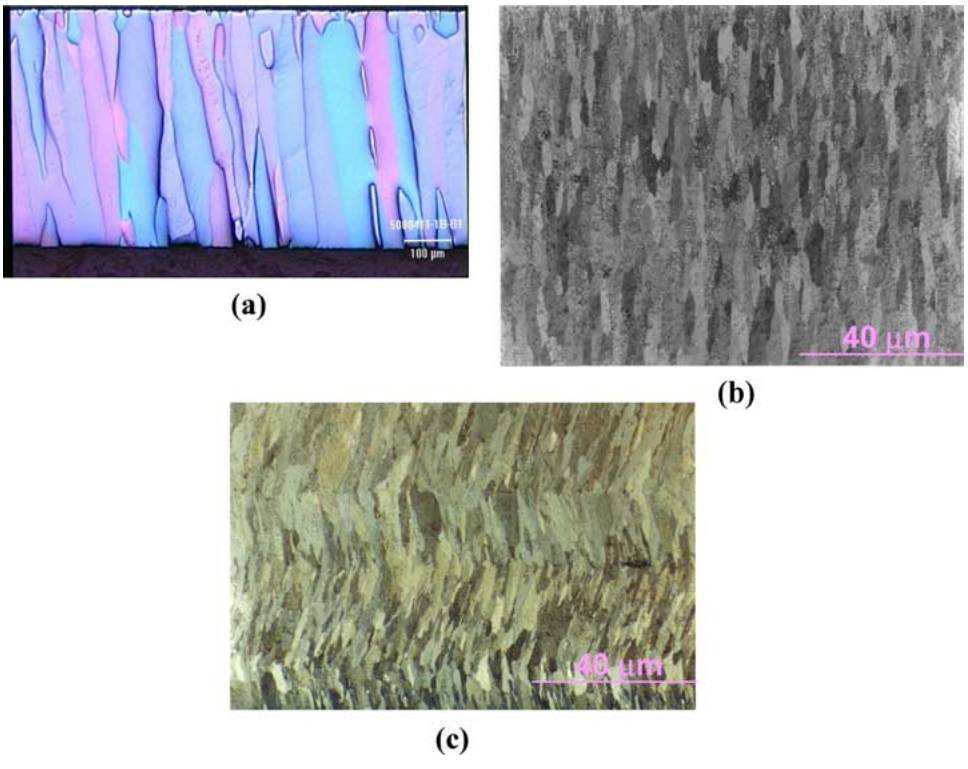

Figure 29 Optical micrograph showing (a) continuous single columnar grains, (b) textured sub-grains and (c) Zig-zag microstructure of Re-plate thickness of 2000 μm deposited on graphite produced by EB-PVD.

Figure 30 (a) Mo-cage used for applying Re coatings on 17-graphite cores and (b) polished Re-coated graphite cores with surface finish $<R_a 8$.

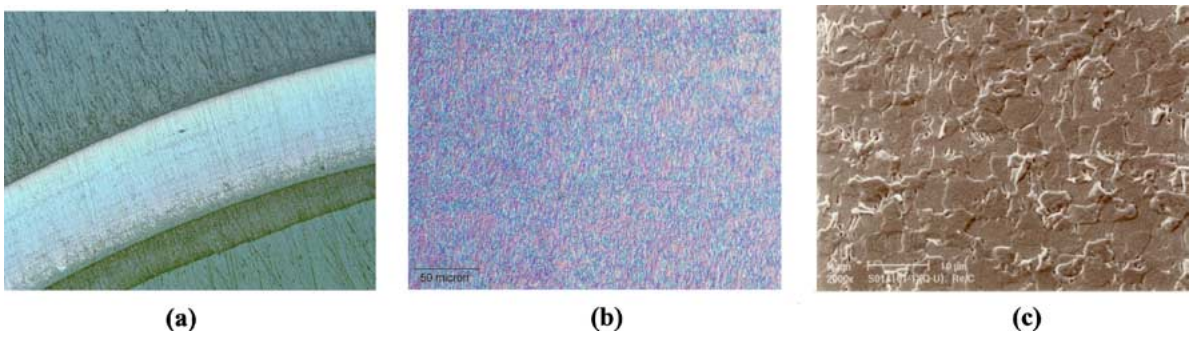

Figure 31 Cross-section of the rhenium-coated graphite core exhibiting dense microstructure with nano and submicron sized grains (a) optical micrograph: low magnification, (b) optical micrograph: high magnification, and (c) SEM micrograph.

4.7.3. Fabrication of rhenium tubes

A similar effort was undertaken in manufacturing of rhenium (Re) tubes with a wall thickness of 150 μm and length of 25 cm. Such tubes were manufactured using Mo tubes as sacrificial mandrels on which rhenium was deposited. Once the Re coating is deposited, the Mo mandrel is removed by chemical dissolution leaving behind the skin of the coating, i.e., rhenium in the tubular form. Currently, Re tubes are manufactured by CVD. The main drawback of this process is that the Re tube contains 2–4 grains through the wall thickness which does not provide adequate number of grains for

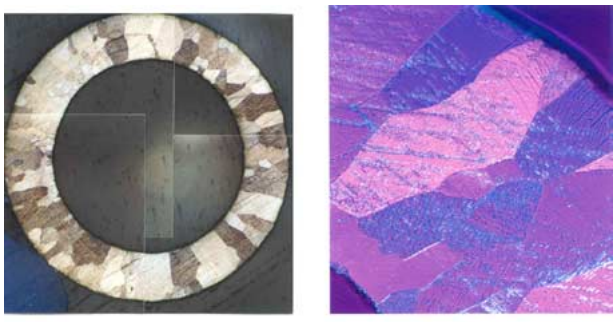

(a) (b)

Figure 32 Cross section of rhenium tube produced by CVD exhibiting 1–3 grains through 150 μm wall thickness (a) low magnification and (b) high magnification.

welding and bending applications (Fig. 32). In addition, there are not enough grains through the wall thickness to accommodate pressure under high-temperature burst tests. Again, CVD process is limited in manufacturing of Re tubes (2–3 tubes at a time).

The shortcoming of CVD process was addressed by exploiting EB-PVD technology. Similarly, Mo mandrel concept was used in manufacturing of Re tubes by IBA, EB-PVD. Tooling concept developed in the manufacturing of Re tube by EB-PVD is displayed in Fig. 33a. Eleven Mo mandrels were mounted simultaneously for applying Re coatings. Mo mandrels were periodically rotated to get uniform coating thickness across the diameter. Mo mandrels were heated indirectly to 1000°C during Re deposition.

The cross section of the rhenium coated Mo mandrel is shown in Fig. 33b. Rhenium coating was very uniform around the Mo tube. Optical microstructure of the coated tube exhibited more than 40–50 grains through the wall thickness that is 10 times more grains than the current CVD process, i.e., nano-grained and submicron grained microstructure was observed through the rhenium wall thickness.

4.7.3.1. Fabrication of net-shaped thruster. Net shaped thruster fabrication was demonstrated using titanium as an evaporant due to the high cost of rhenium. The high flexibility of the EB-PVD process, allowed two thrusters (mirror image) to be fabricated simultaneously during the deposition process (34a and b). In contrast, rhenium thruster is currently made by CVD process and only one thruster is made at a time due to the limited flexibility in the chamber.

4.7.3.2. Manufacturing of nano-flake materials. There is continuous thrust in making nanoflakes of different materials including TiB_2, TiC, TiN, for a wide range of aerospace and military applications. Currently, no technology exists in which nano flakes can be produced at high rates of such materials. Effort was undertaken to demonstrate the proof-of-concept in making nano flakes of TiC. In this effort, TiC ingot was directly evaporated in the EB-PVD chamber. By periodic interruption of evaporant, TiC flakes were produced with sharp interfaces. These flakes were deposited on cold wall/substrate with large CTE mismatch between substrate and the coating. As a combined effect of large CTE mismatch, low temperature deposition and periodic interruption, TiC flakes were produced as shown in Fig. 35. These flakes curled indicating a high mixed residual stress state, as shown in Fig. 35a. In addition, many multiple sharp distinct interfaces were observed through the thickness of the TiC flakes as shown in Fig. 35b. Since TiC is brittle in nature, these flakes were further segmented into small pieces by using applied pressure (Fig. 35c). The thickness of these segmented flakes depends upon the periodicity of vapor cloud interruption, deposition rate, and pressure applied.

4.7.3.3. High-temperature and light-weight radiators and reflectors. There is a significant challenge in the design, development and fabrication of the light weight high temperature radiators for space applications. There are three challenges namely: the radiator should have high emissivity, (especially at elevated temperatures ranging from 1130–1575°C); re-usable, and light weight. In the current design of the advanced propulsion and power system, the radiator is one of the largest and heaviest components, accounting for approximately 25–30% of the total system weight. In the early stage of nuclear space program, SiC material was

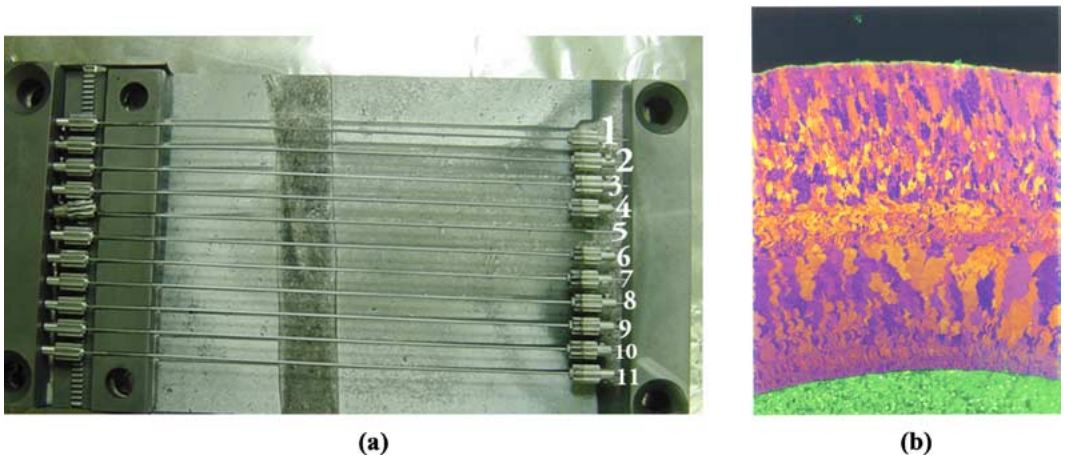

(a) (b)

Figure 33 (a) Tooling used in the fabrication of eleven rhenium tubes simultaneously and (b) optical micrograph of the cross section of rhenium tube produced by EB-PVD exhibiting >40–50 grains throughout the 150 μm wall thickness.

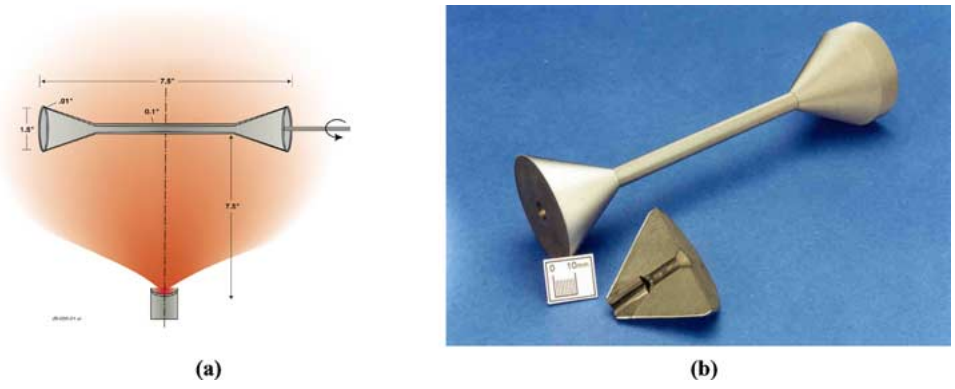

(a) (b)

Figure 34 (a) Diagram showing fabrication of two thrusters simultaneously and (b) two mirror images of titanium-coated graphite mandrel thrusters by EB-PVD with cross section.

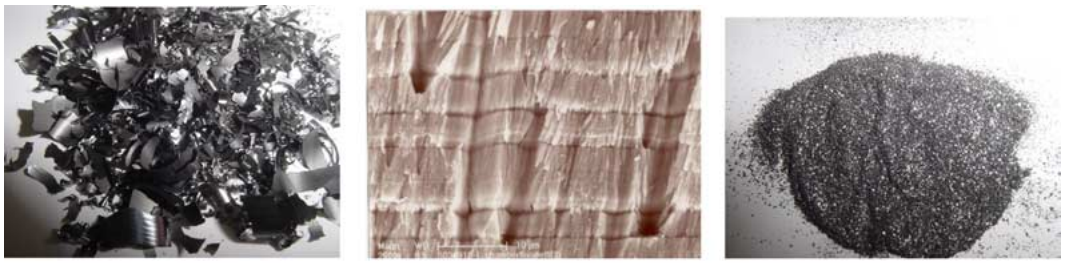

(a) (b) (c)

Figure 35 Photographs of (a) curled TiC flakes produced by EB-PVD, (b) SEM fracture surface of TiC flake showing multiple interfaces, and (c) digital photograph of segmented TiC flakes after applying pressure.

considered as a potential radiator material because of its light weight and high-temperature thermal stability (about 2700°C). However, SiC radiators are vulnerable because of impact and reentry problems associated with erosion, moisture attack and oxidation.

There are only a few candidate materials available for high-temperature reflectors. Effort was undertaken to identify these materials which offer high temperature reflectance and emittance properties. The temperature of interest for pace application ranges from 1400–1600 K. Radiative property of materials is defined in the terms of absorptivity (α), reflectivity (ρ) and transmissivity (τ). Under the first law of thermodynamics,

$$\alpha + \rho + \tau = 1$$

For opaque surface materials, $\tau = 0$

$$\alpha + \rho = 1$$

This is an important property relationship for determining both the absorptivity and reflectivity of opaque surface materials. Under this effort, a thin layer of Ta and Hf-carbide coatings was applied on hexoloy-SiC substrate material.

The corresponding reflectance properties are displayed in Fig. 36. TaC coatings offer excellent thermal reflectance up to 93% at 1 μm wavelength. Similarly, HfC offers higher emittance properties (70%) at 1 μm wavelength as compared with TaC.

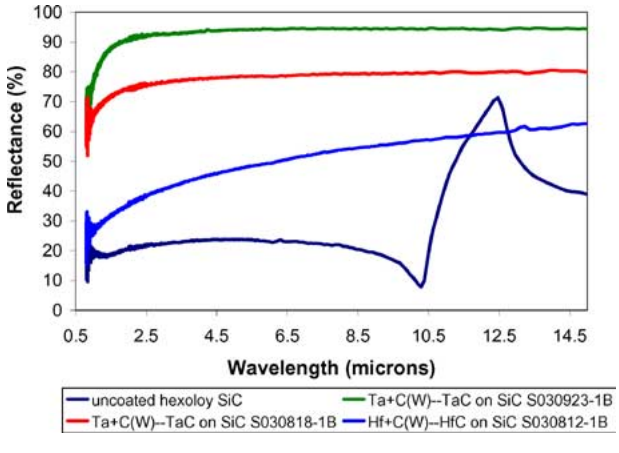

Figure 36 Reflectance measured as a function of wavelength for various coatings deposited by EB-PVD.

5. Summary

This research article demonstrated the versatility of EB-PVD from nano-flakes, coatings, net-shaped forming components. Sequentially or simultaneously co-evaporation of multiple ingots allowed in engineering new coating materials, forming functional graded coatings, components with superior properties including mechanical (hardness and strength) and physical properties such as thermal conductivity and thermal reflectance. Attachment of an ion source to the EB-PVD unit offers additional benefits and flexibility in depositing textured high-density coatings at a relatively low temperature. Processing parameters control the microstructure, physical and mechanical properties, and residual stresses present within the coating.

Acknowledgement

The authors are grateful to various sponsors including US Navy ONR-ManTech Office and NASA for their funding support. Author would also like to express their sincere thanks to various researchers including Farhat Quali Jason Singh, and laboratory staff including Dale D. Donner, Thomas Medill, Dennis McGregor, and Tad Rimmey for their support during the course of experiments. Authors are thankful to Drs. Nam Kang, Steve Copley and Anil Kulkarni for their comments on this review paper.

Appendix

In the spray process, pre-alloyed powder is injected along with a carrier gas through a high-energy source. The coating material (pre-alloyed powder) is transported in the form of molten or semi-molten droplets and directly deposited onto the components. The principle of the process is to feed powder into the plasma where the particles are rapidly heated to their melting point and accelerated to speeds on the order of 300 m/sec (Fig. A1). After a few milliseconds, the molten powder particles strike and flatten on the object surface where they rapidly solidify. The adhesion of the particles to the substrate is mainly a mechanical bond. As a result, the coating exhibits lower mechanical strength including reduce erosion resistant properties (Table V). The properties of coatings depend upon the coating deposition rate and quality, including density, the spray process selected (D-gun, HVOF, plasma-transferred arc processes, etc.), the processing parameters (including combustion fuel used), and the coating and substrate materials used. The high velocity oxy-fuel (HVOF) thermal spraying process uses internal combustion jet (rocket) to generate hypersonic gas velocities (6000 ft/s)-more than five times the speed of sound [133, 134]. Combustion fuels used include propylene, acetylene, propane, hydrogen, and oxygen gases for spraying carbide and non-carbide coating materials. Key parameters that influence the properties of coatings are flame temperature and particle velocity (Table AI and Fig. A2, respectively). There is also a cold spray process (CSP-derived from thermal spray process) which uses a supersonic gas jet (velocity of 5000 km/h) to accelerate fine powders above a critical velocity at which particles impact, deform plastically, and bond to the substrate to form a coating. The uniqueness of CSP is that it does not use any hot flame or plasma during coating deposition process [135]. CSP is more suitable for ductile and low melting materials including Cu, Al, and Ti. A significant advantage of plasma spray processes is the high deposition rate (100–1000 μm/min) and the fact that various metallic and oxide coatings can be applied depending upon the kinetic energy of the particles and flame temperatures. Spray processes have been very successful in applying thick coatings on large components for wear and oxidation resistant applications. A disadvantage of the spray processes is the inability to obtain homogenous, and high-quality dense coatings. It has been reported that even high density coatings of low melting materials including copper-alloys and aluminum cannot be produced by vacuum plasma spray process (Fig. A3). In addition, the surface of the coating is very rough in comparison with CVD or PVD.

Some of the difficulties of the spray process were addressed by the chemical vapor deposition (CVD) process. CVD is defined as a process whereby a reactant gas mixture is passed in a high-temperature reactor to form a solid product in the form of a thin film at the substrate surface (Fig. A4). The CVD coating process takes place between temperatures of 800 and 1200°C,

TABLE AI Spray coating characteristics of 88 wt%WC-12 wt%Co [ ]

	HVOF	D-Gun	Standard plasma	High-velocity plasma
Flame temperature °C (°F)	2760 (5000)	2760 (5000)	11,100 (20,000)	11,100 (20,000)
Gas velocity	Mach 4	Mach 3	Subsonic	Mach 1
DPH300	1050	1050	750	950
Porosity (%)	0	<1	<2	<1
Oxide content (%)	<1	<1	<3	<1
Typical bond strength (psi)	10,000	10,000	8,000	10,000
Thickness limitation (in)	0.06	0.03	0.025	0.015

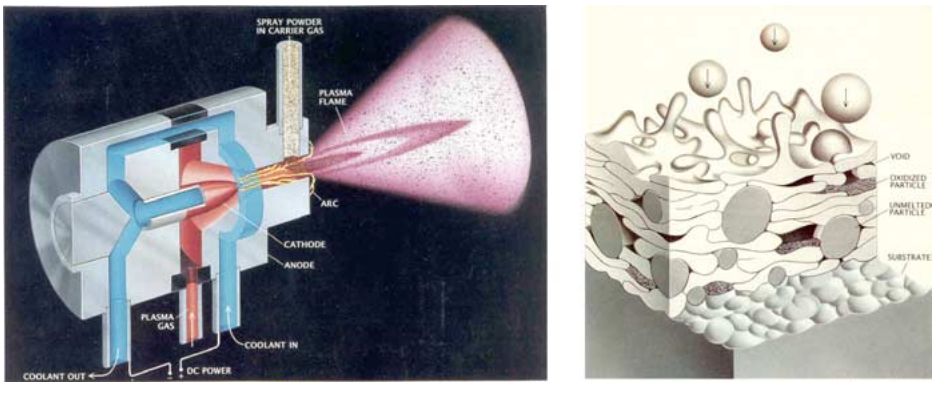

Figure A1 Schematic diagram of plasma spray process and deposition mechanism [136].

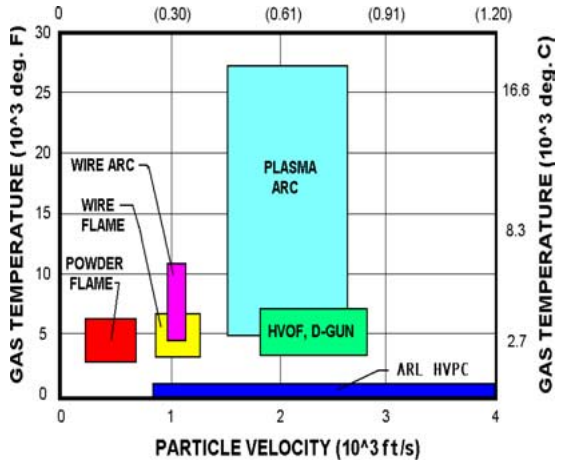

Figure A2 Gas temperature vs. Particle velocity comparison for various spray processes [136].

depending on coating material. Various metallic and ceramic (oxides, carbides, and nitrides) coatings have been deposited at rates of 5–10 μm/h. CVD is very successful in applying dense and wear resistant coatings for cutting tool industry. The disadvantages of the CVD process are that requires high-deposition temperatures (>1000°C); produces chemical waste (such as acids) that is environmentally unacceptable; and deposition rates are usually low (<5 μm/h) for high-quality coatings. The grain size of the coating is relatively large due to high substrate temperature exposed during deposition process, making temperature sensitive substrates difficult to coat. Since, CVD is not a line of sight process, it allows to applying coatings in and out side of the hollow components such as turbine airfoils and vanes.

Some of the shortcomings of the CVD process are addressed by the physical vapor deposition (PVD) processes. The term PVD denotes those vacuum deposition processes where the coating material is evaporated by various mechanisms (resistance heating, high-energy ionized gas bombardment (sputtering), or electron gun) under vacuum, and the vapor phase is transported to the substrate, forming a coating. PVD is a line-of-sight process in which atoms travel from the source material to the substrate in a straight path (Fig. 3). The PVD coating process takes place between temperatures of 100–600°C. Sputtering is one of the most versatile PVD processes available for thin film applications. Various metallic and ceramic (carbides and nitrides) coatings have been applied by this process typically at a rate of a few μm or less per hour. Unlike the CVD process, PVD processes are clean and pollution free. The main disadvantages of PVD processes (with exception of EB-PVD) are the low deposition rates (1–5 μm per hour) and difficulty in applying magnetic materials and oxide coatings efficiently.

In the sputtering processes (Fig. A5), an applied electric field produces plasma of inert-gas ions, which strikes the cathode composed of the source material, and ejects atoms from it. Atoms from the source material are deposited on the surface of the substrate, where they can also combine with reactive gases to form ceramic coatings (e.g., TiN, NbN, etc.). Application of sputtering process is unlimited from cutting tool, micro-electronic, aerospace components to the decorative coating industry. In spite of significant advancements in the various PVD processes (such as cathodic-arc, DC and RF unbalanced-magnetron sputtering), there are still drawbacks in coating quality. For

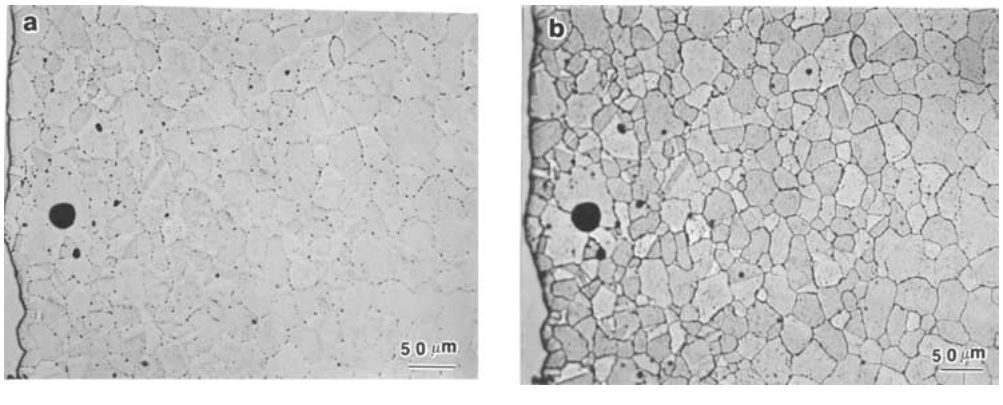

Figure A3 Optical micrograph of NAR-alloy Z^{TM} (Cu-5 wt% Ag) coatings produced by VPS (a) un-etched and (b) etched: showing porosity at grain boundaries [137–139].

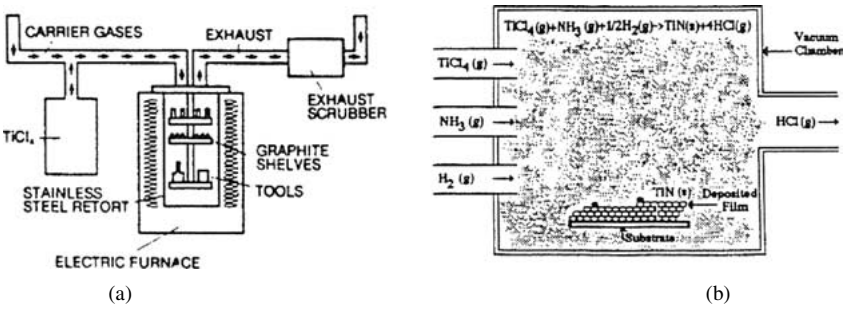

(a) (b)

Figure A4 Schematic diagram of (a) chemical vapor deposition system, (b) CVD chamber, and surface microstructure of a typical TiN coating [140].

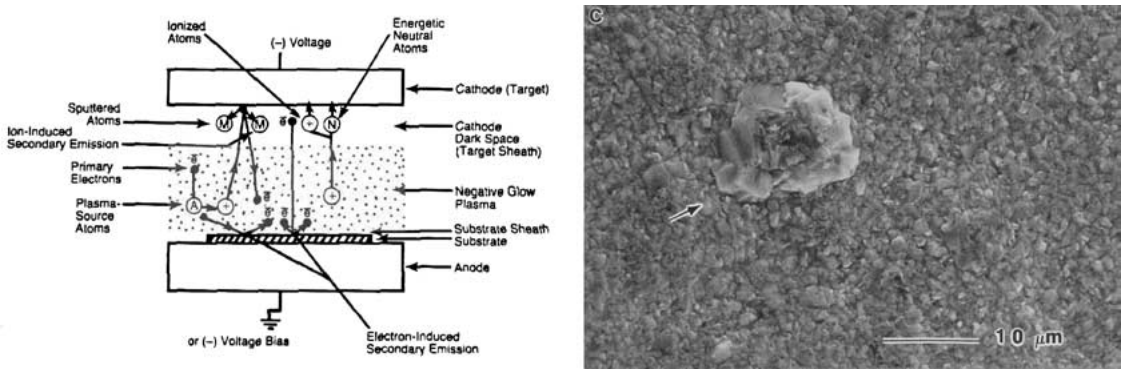

Figure A5 Schematic diagram of sputtering mechanism and SEM photograph of TiN deposited by sputtering [141].

example, the cathodic-arc PVD process produces liquid droplets or macro-particles of metals, 1 to 15 μm in size, during the evaporation of the target material. These molten particles can be entrapped in the growing film, resulting in inhomogeneity in the microstructure and detrimental physical properties.

Ion implantation is not a deposition process, but rather a surface modification process in which appropriate atoms are embedded in a material through high-energy beams. High-energy ions are produced in an accelerator and directed on the surface of the substrate. A high-energy ion implanter (1–10 MeV) is required for deep penetration ($\sim$5 μm). Ionized particles enter into the substrate with kinetic energies four to five orders of magnitude greater than the binding energy of the solid by a collision mechanism. The principal application of ion implantation has been in the electronic industries. Typical application of ion implantation is in the bearing, gear, and biomedical industries. The main disadvantage of the ion implantation process is the limited depth of penetration into the substrate ($<$5 μm) and the long processing times.

Ion plating is a derivative of ion implantation in which the substrate is made the cathode and the source material is thermally evaporated before being partially ionized and accelerated to the substrate (cathode). By proper selection of materials and gas, carbides, nitrides, and oxides can be deposited. Potential applications of ion plating are in tooling industries and certain aircraft components. The disadvantages of the above mentioned PVD processes can be addressed by the ion beam assisted, EB-PVD process.

References

1. J. SOBOTA, G. SORENSEN, H. JENSEN, Z. BOCHNICEK and V. HOLY, *Surf. Coat. Techn.* **142–144** (2001) 590.
2. K. C. CHIN, A. GOHEL, H. I. ELIM, W. JI, G. L. CHONG, K. Y. LIM, C. H. SOW and A. T. S. WEE, *Chem. Phys. Lett.* **383**(1/2) (2004) 72.
3. M. BROGREN, G. L. HARDING, R. KARMHAG, C. G. RIBBING, G. A. NIKLASSON and L. STENMARK, *Thin Solid Films* **370**(1/2) (2000) 268.
4. Q. XIANG, Y. ZHOU, B. S. OOI, Y. L. LAM, Y. C. CHAN and C. H. KAM, *ibid.* **370**(1/2) (2000) 243.
5. H. HOLLECK, "Design of Nanostructured Thin Films for Tribological Applications," TMS Conference Proceedings on Surface Engineering: Science and Technology I, edited by A. Kumar, Y. W. Chung, J. J. Moore and J. E. Smugeresky (1999) p. 207.
6. J. R. NICHOLLS, K. J. LAWSON, D. S. RICKERBY and P. MORRELL "Advanced Processing of TBC for Reduced Thermal Conductivity," AGARD SMP Meeting on "Thermal Barrier Coatings" Aalborg, Denmark, 15–16, Oct. 1997, p. 6-1 to 6–7.
7. R. A. MILLER, "Thermal Barrier Coatings for Aircraft Engines-History and Directions," Thermal Barrier Coating Workshop, NASA CP 3312, 1995, p. 17.
8. O. UNAL, T. E. MITCHELL and A. H. HEUER, *J. Amer. Ceram. Soc.* **77**(4) (1994) 984.
9. R. A. MILLER, *Surf. Coat. Techn.* **30** (1987) 1.
10. J. SINGH, D. E. WOLFE and JASON SINGH, *J. Mater. Sci.* **37** (2002) 3261.
11. K. L. CHOY, *Prog. Mater. Sci.* **48**(2) (2003) 57.
12. S.V. BATTY, T. RICHARDSON, P. PETCOCK and L. RAMAN, *Thin Solid Films* **266**(2) (1995) 96.
13. D. E. WOLFE, Thesis 1996MSWolfe DE, Penn State University, 2001.
14. R. BUNSHAH (ed.) "Handbook of Deposition Technologies for Films and Coatings" (Noyes Publications, Park Ridge, N.J., 1994).
15. M. HOCKING, "Metallic and Ceramic Coatings, Longman Scientific and Technical" (John Wiley and Sons Inc., 1989).
16. R. J. Hill (ed.), "Physical Vapor Deposition," Temescal, a Division of the BOC Group, Inc., Berkeley, CA (1986).
17. R. MCINTYRE, *Mater. Proc.* **8** (1996) 455.
18. J. SINGH, *J. Mater. Sci.* **29** (1994) 5232.
19. YONG-JUN TAN and KIM YONG LIM, *Surf. Coat. Techn.,* **167**(2/3) (2003) 255.
20. S. SAFAIE, L. F. POCHET and P. HOWARD, *ibid.* **94/95**(1/3) (1997) 70.
21. SVEND S. ESKILDSEN, *ibid.* **116–119** (1999) 18.
22. W. BEELE, G. MARIJNISSEN and A. VAN LIESHOUT, *ibid.* **120/121** (1999) 61.
23. P. FAUCHAIS and A. VARDELLE, *Intern. J. Therm. Sci.* **39**(9–11) (2000) 852.
24. J. R. PIERCE, "Theory of Design of Electronic Beams," D. Van Nostrand Company Inc., New York, New York (1954).
25. D. E. WOLFE and J. SINGH, *J. Mater. Sci.* **33** (1998) 3677.
26. H. HOLLECK "Design of Nanostructured Thin Films for Tribological Applications," TMS Conference Proceedings on Surface Engineering: Science and Technology I, edited by A. Kumar, Y. W. Chung, J. J. Moore and J. E. Smugeresky (1999) p. 207.
27. D. E. WOLFE, M. MOVCHAN and J. SINGH, "Architecture of Functionally Gradient Ceramic-Metallic Coatings By EB-PVD for High Temperature Applications," Proceedings of Proceeding of Advances in Coating Technologies, at TMS Annual Meeting at Orlando, edited by C. R. Clayton and J. K. Hirvonen (TMS, 1997) p. 93.
28. D. E. WOLFE J. SINGH and K. NARASIMHAN, *J. Surf. Coat. Techn.* **165** (2003) 8.
29. DOUGLAS E. WOLFE, "Synthesis and characterization of TiC, TiBCN, TiB_2/TiC, and TiC/CrC multilayer coatings by reactive and ion beam-assisted, electron beam-physical vapor deposition (EB-PVD)" Thesis 2001D Wolfe DE, Penn State University, University Park, PA, 2001.
30. O. AUCIELLO, M. S. AMEEN, A. R. KRAUSS, A. I. KINGON and D. J. LICHTENWALNER, "Surface Modification Technologies IV," edited by T. S. Sudarshan, D. G. Bhat

and M. Jeandin (The Minerals, Metals and Materials Society, PA, 1991) p. 109.
31. J. L. VOSSEN and J. J. CUOMO, "Thin Film Processes" (Academic Press, Inc., 1978) p. 11.
32. W. ENSINGER, A. SCHROER and G. K. WOLF, *Nucl. Instr. Meth. Phys. Res.* B **80/81** (1993) 445.
33. A. KOLITSCH, E. HENTSCHEL and E. RICHTER, *ibid.* **80/81** (1993) 258.
34. J. ARNALT, J. DELAFOND, C. TEMPLIER, J. CHAUMONT and O. ENEA, *ibid.* **80/81** (1993) 1384.
35. W. ENSINGER, R. EMMERICH and B. ENDERS, in "Surface Modification Technologies IV," edited by T. Sudarshan and D. Bhat (The Minerals, Metals & Materials Society, PA, 1993) p. 859.
36. B. HAYWOOD, *Adv. Mater. Proc.* **12** (1990) 35.
37. R. EMMERICH, B. ENDERS and W. ENSINGER, Surface Modification Technologies VI, edited by Sudarshan (The Minerals, Metals & Materials Society, PA, 1993) p. 811.
38. J. HIRVONEN, *Mater. Sci. Reports* **6** (1991) 215.
39. G. WOLF and W. ENSINGER, *Nucl. Instr. Meth. Phys. Res.* B **59/60** (1991) 173.
40. J. HIRVONEN, *Annu. Rev. Mater. Sci.* **19** (1989) 401.
41. G. WOLF, *J. Vac. Sci. Technol.* A **10**(4) (1992) 1757.
42. H. KAUFMAN, R. S. ROBINSON and W. E. HUGHES, "Characteristics, Capabilities, and Applications of Broad-Beam Sources" (Commonwealth Scientific Corporation, Alexandria, VA, 1987) p. 1.
43. K. KUWAHARA, T. SUMOMOGI and M. KONDO, *Thin Solid Films* **78** (1981) 41.
44. F. A. QULI, Thesis 1999d Quli FA, Penn State University, 1999.
45. L. A. STELMACK, C. T. THURMAN and G. R. THOMPSON, *Nucl. Instru. Meth. Phys. Res.* B **37/38** (1989) 787.
46. H. OETTEL and R. WIEDEMANN, *Surf. Coat. Techn.* **76/77** (1995) 265.
47. I. C. NOYAN, T. C. HUANG and B. R. YORK, *Crit. Rev. Solid State Mater. Sci.* **20**(2) (1995) 125.
48. A. PEITER and H. WERN, *Strain*, Aug. (1987) 103.
49. R. HULL, J. C. BEAN, F. ROSS, D. BAHNCK and L. J. PETICOLAS, *Mater. Res. Soc. Symp. Proc.* **239** (1992) 379.
50. J. H. JE, D. Y. NOH, H. K. KIM and K. S. LIANG, *J. Appl. Phys.* **81**(9) (1997) 6126.
51. G. KNUYT, C. QUAEYHAEGENS, J. D'HAEN and L. M. STALS, *Thin Solid Films* **258** (1995) 159.
52. W. ENSINGER, *Nucl. Instr. Meth. Phys. Res.* B **106** (1995) 142.
53. C. QUAEYHAEGENS, G. KNUYT, J. D'HAEN and L. M. STALS, *Thin Solid Films* **258** (1995) 1710.
54. B. RAUSCHENBACH and K. HELMING, *Nucl. Instr. Meth. Phy. Res.* B **42** (1989) 216.
55. M. KIUCHI, K. FUJII, T. TANAKA, M. SATOU and F. FUJIMOTO, *ibid.* B **33** (1988) 649.
56. J. W. GERLACH, U. PRECKWINKEL, H. WENGENMAIR, T. KRAUS and B. RAUSCHENBACH, *Appl. Phys. Lett.* **68**(17) (1996) 2360.
57. W. ENSINGER and B. RAUSCHENBACH, *Nucl. Instr. Meth. Phys. Res.* B **80/81** (1993) 1409.
58. H. JIANG, K. TAO and H. LI, *Thin Solid Films* **258** (1995) 51.
59. Y. NAKAMURA, Y. WATANABE, S. HIRAYAMA and Y. NAOTA, *Surf. Coat. Techn.* **76/77** (1995) 337.
60. Y. ANDOH, K. OGATA, H. YAMAKI and S. SAKAI, *Nucl. Instr. Meth. Phys. Res.* B 39 (1989) 158.
61. T. ROTH, K. H. KLOOS and E. BROSZEIT, *Thin Solid Films* **153** (1987) 123.
62. D. E. WOLFE and J. SINGH, *J. Mater. Sci.* **34** (1999) 2997.
63. R. NIMMAGADDA and R. F. BUNSHAH, *Thin Solid Films* **45** (1977) 477.
64. B. E. JACOBSON, C. V. DESHPANDEY, H. J. DOERR, A. A. KARIM and R. F. BUNSHAH, *ibid.* **118** (1984) 285.
65. J. E. SUNDGREN, *ibid.* **128** (1985) 21.
66. *Idem.*, *ibid.* **105** (1983) 367.
67. D. M. MATTOX, in "Ion Implantation and Plasma Assisted Processes," edited by R. F. Hochman, H. Solnick-Legg and K. O. Legg (ASM International, Metals Park, OH, 1988) p. 9.
68. H. HOLLECK, M. LAHRES and P. WOLL, *Surf. Coat. Techn.* **41** (1990) 179.
69. J. E. SUNDGREN and L. HULTMAN, "Materials and Processes for Surface and Interface Engineering," edited by Y. Pauleau (Kluwer Academic Publishers, Netherlands, 1995) p. 453.
70. H. HOLLECK, "Surface Engineering: Science and Technology I," edited by A. Kumar, Y. W. Chung, J. J. Moore and J. E. Smugeresky (The Minerals, Metals, & Materials Society, Warrendale, PA, 1999) p. 207.
71. P. BARNA and M. ADAMIK, "Growth Mechanism of Polycrystalline Thin Films", Science and Technology of Thin Films, edited by F. C. Matacotta and G. Ottaviani, (World Scientific Publishers, New Jersey, 1995) p. 1.
72. P. B. BARNA, G. BARCZA, L. TOTH, G. VINCZE, A. BERGAUER and H. BANGERT, *Surf. Coat. Techn.* 57 (1993) 7.
73. P. B. BARNA, "Diagnostics and Applications of Thin Films," edited by L. Eckertova and T. Ruzicka (Charles University, Prague, Czechoslovakia, 1991) p. 295.
74. A. C. RAGHURAM and R. F. BUNSHAH, *J. Vacuum Sci. Techn.* **9**(6) (1972) 1389.
75. B. A. MOVCHAN and DEMICHISEN, *Fitz. Metal. Metall.* **28**(4) (1969) 653.
76. J. A. THORNTON, *J. Vacuum Sci. Techn.* **11**(4) (1974) 666.
77. *Idem.*, *ibid.* **12**(4) (1974) 830.
78. R. MESSIER, A. P. GIRI and R. A. ROY, *ibid.* **2**(2) (1984) 500.
79. H. HABERLAND, M. MOSELER, Y. QIANG, O. RATTUNDE, Y. THURNER and T. REINERS, "Energetic Clusters Impact: New features in Deposition Technology," 2nd International Conference on Beam Processing of Materials, ASM international, edited by J. Singh, S. M. Copley and J. Mazumder, Oct. (1995) p. 69.
80. M. LEVIT, I. GRIMBERG and B. Z. WEISS, *Mater. Sci. Engng.*, A **206** (1996) 3038.
81. D. S. RICKERBY and P. J. BURNETT, *Thin Solid Films* **157** (1988) 195.
82. F. A. QULI and J. SINGH, *J. Mater. Sci. Engng.* B (1999) 139.
83. V. E. BAUER " Fibre Texture," Transaction of 9th National Vacuum Symposium (1962) p. 35.
84. VAN DER DRIFT "Evolutionary Selection, a Principal Governing Growth Orientation in Vapor-Deposited Layers," Philips Research Report, (1967) Vol. 22, p. 267.
85. P. L. SHAH, *IEEE Trans. Electron. Dev.* ED-26 (1979) 631.
86. D. SMITH, "Thin-Film Deposition Principles and Practice" (McGraw-Hill, Inc., New York, New York, 1995) p. 431.
87. F. A. Quli, "Molybdenum Metallization and Step Induced Defects in Active Matrix Liquid Crystal Display," Ph.D. thesis, Penn State University, University Park, PA, 1999.
88. W. SPROUL, *Cutt. Tool Engng.* (1994) 52.
89. G. SANDHU, S. MEIKLE and T. DOAN, *Appl. Phys. Lett.* **63**(3) (1993) 240.
90. T. ARAI, H. GUJITA and K. OGURI, Thin Solid Films **165** (1988) 139.
91. J. STIMMELL, *J. Vac. Sci. Technol.* B **4**(6) (1986) 1377.
92. G. DIXIT, C. WEI, F. LIOU and H. ZHANG, *Appl. Phys. Lett.* **62**(4) (1993) 357.
93. S. ROHDE, Y. KIM and R. DEANGELIS, *J. Electr. Mater.* **22**(11) (1993) 1327.
94. X. CHU, M. S. WONG, W. D. SPROUL, S. L. RHODE and S. A. BARNETT, *J. Vac. Sci. Technol.* A **10** (1992) 1604.
95. X. CHU and S. A. BARNETT, *J. Appl. Phys.* **77** (1995) 4403.
96. K. J. MA, A. BLOYCE and T. BELL, *Surf. Coat. Techn.* **76/77** (1995) 297.
97. H. HOLLECK and M. LAHRES, *Mater. Sci. Engng.* A **140** (1991) 609.
98. H. HOLLECK, M. LAHRES and P. WOLL, *Surf. Coat. Techn.* **41** (1990) 179.
99. J. E. SUNDGREN and L. HULTMAN, in "Materials and Processes for Surface and Interface Engineering," edited by Y. Pauleau (Kluwer Academic Publishers, Netherlands, 1995) p. 453.
100. H. HOLLECK and H. SCHULTZ, *Surf. Coat. Techn.* **36** (1988) 707.
101. D. E. WOLFE and J. SINGH, *J. Mater. Sci.* **37** (2002) 3777.

102. *Idem.*, *Surf. Coat. Techn.* **124** (2000) 142.
103. D. ZONG, E. SUTTER, J. J. MOORE, G. G. MUSTOE, E. A. LEVASHOV and J. DISAM, *Thin Solid Films* **398/399** (2001) 320.
104. D. E. WOLFE, J. SINGH and K. NARASIMHAN, *Surf. Coat. Techn.* **160** (2002) 206.
105. M. SCHROEDER and R. UNGER, *Adv. Mater. Proc.* **8** (1997) 19.
106. J. W. DINI, *Mater. Manufact. Proc.* **12** (1997) 437.
107. B. C. OBERLANDER and E. LUGSCHEIDER, *Mater. Sci. Techn.* **8** (1992) 657.
108. D. W. PARKER and G. L. KUTNER, *Adv. Mater. Proc.* **4** (1991) 68.
109. J. SINGH, *ibid.* **11** (1996) 32.
110. J. SINGH, "Hard Coatings Evaluation by Plasma Spray Processes," private communication (2003).
111. D. E. WOLFE and J. SINGH, "Functionally Graded Ceramic/Metallic Coatings for Gas Turbine Components by High Energy Beams for High Temperature Applications," NATO-Advanced Study Institute Series Proceedings on "Protective Coatings and Thin Films," edited by Y. Pauleau and P. Barna, (1996) Vol. 21, p. 441.
112. DOUGLAS E. WOLFE and J. SINGH, "Effect of Substrate Rotation and Vapor Incidence Analysis on Microstructure of Thermal Barrier Coatings Deposited by EB-PVD," Technical Memorandum 97, Applied Research Laboratory, Penn State University (Feb. 1996).
113. J. SINGH, *Surf. Engng. Bull.* **7** (1996) 8.
114. D. E. WOLFE, M. MOVCHAN and J. SINGH, "Architecture of Functionally Gradient Ceramic-Metallic Coatings by EB-PBD for High Temperature Applications," in Proceedings of Advances in Coating Technologies, edited by C. R. Clayton and J. K. Hirvonen, (TMS Annual Meeting in Orlando, Fl, 1997) p. 93.
115. R. A. MILLER, *Surf. Coat. Techn.* **309** (1987) 01.
116. K. S. RAVICHANARAN, K. AN, R. E. DOTTON and S. L. SEMIATIN, *J. Amer. Ceram. Soc.* **82**(30) (1999) 673.
117. JOGENDER SINGH DOUGLAS E. WOLFE, ROBERT MILLER, JEFF ELDRIDGE and DONG-MING ZHU, "Thermal Conductivity and Thermal Stability of Zirconia and Hafnia Based Thermal Barrier Coatings by EB-PVD for High Temperature Applications," II International Materials Symposium Universidade Nova de Lisboa, Campus da Caparica, Portugal, April 14–16, 2003.
118. D. E. WOLFE, J. SINGH, R. MILLER, J. ELDRIDGE and D. ZHU, *J. Surf. Coat. Techn.* accepted.
119. J. SINGH and D. E. WOLFE, "Tailored Microstructure and Composition of Advanced Thermal Barrier Coatings with Low Thermal Conductivity and High Reflectance by EB-PVD for High Temperature Applications," Technical Report, Applied Research Laboratory, Penn State University (Feb., 2003).
120. D. V. RIGNEY, R. VIGUIE, D. J. WARTMAN and D. W. SKELLY, *J. Therm. Spray Techn.* **6** (1997) 167.
121. U. SCHULTZ, T. KRELL, U. LEUSHAKE and M. PETERS, "Graded Design of EB-PVD Thermal Barrier Coatings System," Proc. AGARD Workshop on Thermal Barrier Coatings," Aalborg, DK, Oct. 15–16, 1997.
122. YONG-HO SOHN "Characterization and Life Prediction of Physical Vapor Deposited Partially Stabilized Zirconia Thermal Barrier Coatings," Ph.D. thesis, Worcester Polytechnic Institute, MA, 1993.
123. D. E. WOLFE and J. SINGH, "Effect of Substrate Rotation and Vapor Incidence Angles on Microstructure of Thermal Barrier Coatings Deposited by EB-PVD," Internal Report # 98-109, Applied Research Laboratory, Pennsylvania State University (December, 1997).
124. M. MOVCHAN and J. SINGH, "Development of Multicomponent Coatings by EB-PVD Functionally Graded Ceramic Coatings, in Proceedings of the EB-PVD Workshop at Penn State University, edited by J. Singh and Boris Movchan (Sept., 1996).
125. D. E. GLASS, RAVI N. SHENOY, Z. WANG and M. HALBIG "Effectiveness of Diffusion Barrier Coatings for Mo-Re Embedded in C/SiC and C/C," NASA/TM (2001) p. 1264.
126. J. SINGH and D. WOLFE, "Functionally Graded Nano-Grain Re $\rightarrow$ Zr $\rightarrow$ ZrN and Re $\rightarrow$ Hf $\rightarrow$ HfN Coatings on Re-Mo Alloy Substrate by Ion Beam Assisted, Electron Beam-Physical Vapor Deposition," Final Report, Applied Research Laboratory, Penn State University (Jan., 2003).
127. A. J. SHERMAN, R. H. TUFFIAS and R. B. KAPLAN, *J. Metals* July (1991) 20.
128. B. D. REED, J. A. BIAGLOW and S. SCHNEIDER, Iridium—Coated Rhenium Radiation Cooled Rockets, NASA Technical Memorandum Number 107453. Feb. (1997) p. 1.
129. T. LEONHARDT, M. HAMISTER, J. CARLEN, J. BIAGLOW and B. REED, Near net shape powder metallurgy rhenium thruster, Conference proceedings of 36th American Institute of Aeronautics and Aeronautics, Huntsville, AL, 17–19 July (2000) p. 1.
130. J. O. MILEWSKI, D. J. THOMA, J. C. FONSECA and G. K. LEWIS, *Mater. Manuf. Proc.* **13** (1998) 719.
131. J. SINGH and D. E. WOLFE, *J. Adv. Mater. Proc.* **160** (2002) 39.
132. *Idem.*, *J. Adv. Mater. Manuf. Proc.* (in press, 2004).
133. D. L. GILMORE, R. C. DYKHUIZEN, R. A. NEISER, T. J. ROEMER and M. F. SMITH, *J. Thermal Spray Tech.* **8**(4) (1999) 576.
134. D. L. GILMORE, R. A. NEISER and R. C. DYKHUIZEN, "Modeling The Critical Velocity for Deposition in the Cold Spray Process," Honorary Session for Professor Herbert Herman on Spray Coating Formation and Evaluation," MRS Fall Meeting, Boston, MA (Nov., 1999).
135. M. F. AMATEAU and T. EDEN "High Velocity Particles Consolidation Technology," Technical Article in Institute of Manufacturing and Sustain Technology-Quarterly Report Number 2 (2000).
136. D. W. PARKER and G. L. KUTNER, *Adv. Mater. Proc.* **4** (1991) 68.
137. J. SINGH, G. JERMAN, B. BHAT and R. POORMAN, "Microstructural Stability of Wrought, Laser and Electron Beam Glazed NARloy-Z at Elevated Temperatures," NASA Technical Report #108431 (1993) p. 1.
138. J. SINGH, G. JERMAN, B. N. BHAT and R. POORMAN, "Microstructural Evolution of NARloy-Z At Elevated Temperature," NASA Technical Report # 108419 (1993) p. 1.
139. J. SINGH, G. GERMAN, R. POORMAN, B. N. BHAT and A. K. KURUVILLA, *J. Mater. Sci.* (1997) 3891.
140. n.a., Technical/Applications Guide, Scientific Coatings Inc., n.p., n.d., 1–20.
141. F. SEQUEDA, *J. Metals* (1986) 55.

Received 1 September 2003
and accepted 30 June 2004